Supporting Information for

Promotion Mechanism for the Growth of CO2 Hydrate with Urea from Molecular Dynamics Simulations

Po–Wei Wang[a], David T. Wu[b] and Shiang-Tai Lin[a]*

[a]Department of Chemical Engineering, National Taiwan University, Taiwan

[b]Department of Chemistry and Department of Chemical and Biological Engineering,

Colorado School of Mines, USA

1. Method

All molecules dynamics simulations (MD) were carried out using open source software GROMACS 4.5.5 [1]. The Lennard-Jones potential [2] and Coulomb interaction were calculated with a cutoff of 9.5 Å. The Particle-Mesh Ewald (PME) [3] and dispersion corrections [4] were applied for calculating the long-range Coulomb and van der Waals contributions to energy and pressure. The Nose−Hoover thermostat [5] was used for temperature control with τ_t = 1 ps and the Parrinello−Rahman barostat [6] was used for pressure control with τ_P = 10 ps. The TIP4P-ICE potential [7] was used for water, EPM2 model [8] for CO_2, and OPLS-AA model [9, 10] for urea. For interactions between water and urea, and interactions between water and CO_2 a scaling factor was added, i.e., $\varepsilon_{ij} = \chi(\varepsilon_{ii}\varepsilon_{jj})^{1/2}$ with χ being set to 1.1. Further details about force field setting are provided in the Table S 1 to Table S 6.

The force field parameters of TIP4P-ICE model for water [7], EPM2 model for CO_2 [8], and OPLS-AA model for urea [9, 10] are summarized in Table S 1. The geometric combination rule ($\varepsilon_{ij} = (\varepsilon_{ii}\varepsilon_{jj})^{1/2}$ and $\sigma_{ij} = (\sigma_{ii}\sigma_{jj})^{1/2}$) is used for the Lennard - Jones parameters between unlike atoms. However, we found the melting point of CO_2 hydrate, the CO_2 solubility in water, and the urea solubility in water from simulation are lower than experiment data. Therefore, a scaling factor was added for water – urea and water – CO_2 , i.e., $\varepsilon_{ij} = \chi(\varepsilon_{ii}\varepsilon_{jj})^{1/2}$ [11] [12], to enhance these intermolecular interactions. The optimal values were found to be $\chi_{CO2\text{-}water}$ = 1.1 and $\chi_{urea\text{-}water}$ = 1.1, as illustrated in the next section.

Table S 1. Force field parameters.

Molecule	Atom	ε (kJ/mol)	σ (nm)	q (e)
water	O	0.881949	0.316685	0.0000
	H	0	0	0.5897
	MW	0	0	-1.1794
CO_2	C	0.233865	0.2757	0.6512
	O	0.669335	0.3033	-0.3256
urea	C	0.43932	0.375	0.142
	O	0.87864	0.296	-0.390
	N	0.71128	0.325	-0.542
	H	0	0	0.333

2. Scaling factor between water and CO_2 ($\chi_{CO2\text{-}water}$)

To determine the suitable scaling factor for the interaction between water and CO_2, melting point of CO_2 hydrate, and CO_2 solubility in water were measured with $\chi_{CO2\text{-}water}$ = 1.0 and 1.1. The initial structure used for melting point at 45 bar is the same as Figure 1 of the main text. The results are shown in Table S 2. The initial structure for CO_2 solubility is shown in Figure S 1. The system contains two slabs: a liquid phase of 1500 water molecules and a gas phase of 750 CO_2 molecules. The simulations were conducted at 50 bar and 298 K for 250 ns. The solubility was determined from the average number of CO_2 molecules in the water phase in the final 200 ns. The results are shown in Table S 3.

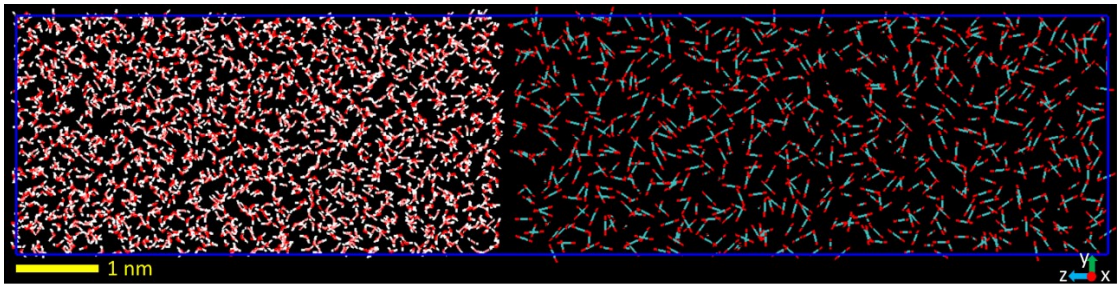

Figure S 1. The initial structure for CO_2 solubility simulation.

Table S 2. The CO_2 hydrate melting point at 45 bar using different values of $\chi_{CO2\text{-}water}$

$\chi_{CO2\text{-}water}$	1.0	1.1	Exp [13]
melting point (K)	275	285	283

Table S 3. The CO_2 solubility in water at 50 bar and 298 K using different values of $\chi_{CO2\text{-}water}$

$\chi_{CO2\text{-}water}$	1.0	1.1	Exp [14]

solubility (mol frac.)	0.0149	0.0295	0.0216

3. Scaling factor between water and urea ($\chi_{urea\text{-}water}$)

The scaling factor for the interaction between water and urea was determined based on urea solubility in water, heat of dissolution of urea, and thermodynamic inhibition of CO_2 hydrate with the presence of urea with $\chi_{urea\text{-}water}$ = 1.0, 1.1, and 1.2. The scaling factor for water-CO_2 interactions, $\chi_{CO2\text{-}water}$, is set to 1.1 in this section. The simulations were conducted at 1 bar and 298 K.

There are two ways to measure urea solubility in water. One is to start from an undersaturated solution (dissolution approach), and the other is from a supersaturated solution (growing approach). For the dissolution approach (initial system shown in Figure S 2), the system contains two slabs: a solid phase of 5 × 5 × 20 urea crystal unit cells (1000 urea molecules) and a liquid phase of 2000 water molecules with 100 urea molecules (X_{urea} = 0.0476). (Note the experimental equilibrium urea concentration is X_{urea} = 0.263 [15]) The dissolution of urea from the crystalline phase needs to overcome an energy barrier of creating a defect on the crystal surface layer. Once the defect forms, the surface layer dissolves quickly. The defect creation rate can be very slow when the urea concentration approaches to its solubility. Therefore, the growing approach was also used to determine the upper bound of solubility. The initial structure (Figure S 3) contains two slabs: a solid phase of 5 × 5 × 5 urea crystal unit cells (250 urea molecules), and a liquid phase of 2000 water molecules and 850 urea molecules (X_{urea} = 0.298). The urea crystal only grows about one uncompleted layer in the z-direction on both sides of the urea crystal because the rate-limiting step for crystallization is the removal of surface defects. It takes more time to remove of surface defects than to create surface defects. These phenomena were also reported and discussed in-depth in Piana's work [16]. The dissolution and growing approaches thus gave us the upper and lower bounds of urea solubility in water. The results are shown in Table S 4.

All the urea crystal used in the simulation was created with the urea crystal parameter from Swaminathan et al [17]. The 001 surface is set to the z direction for dissolution and growing simulations since it is the fastest surface for growing in experiment [18].

The heat of dissolution of urea is determined from the difference in energy of three systems. One is a 5 × 5 × 5 urea crystal (250 urea molecules). Second is a pure water system of 1100 water molecules. The third is a homogenous urea solution of 100 urea molecules and 900 water molecules (X_{urea} = 0.1). Simulations were conducted at 1 bar and 298 K (NPT) for 10 ns. The results are shown in Table S 5.

The thermodynamic inhibition effect of CO_2 hydrate by urea is determined using a three-phase model (Figure S 4) consisting four slabs of materials. The 2×2×2 unit cell

of fully occupied structure I CO_2 clathrate hydrate (consisting of 368 water molecules and 64 CO_2) is sandwiched by two slabs of liquid water (consisting of 736 water molecules, and 82 urea molecules (X_{urea} = 0.1)). The two liquid water slabs are separated by a gas phase of 256 CO_2 molecules. The results are summarized in Table S 6.

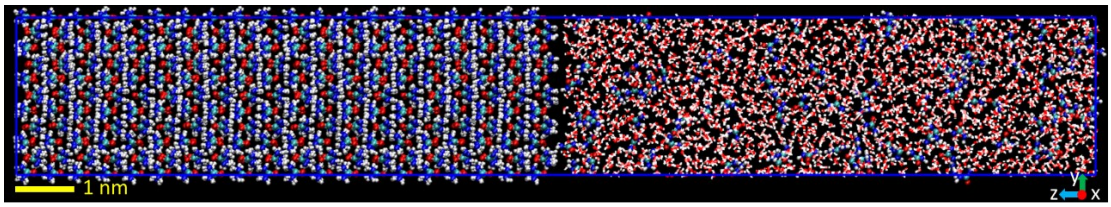

Figure S 2. The initial structure used for urea solubility simulation from dissolution approach.

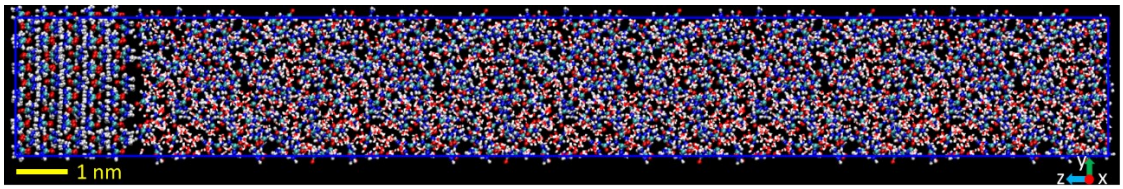

Figure S 3. The initial structure for urea solubility simulation from growing approach.

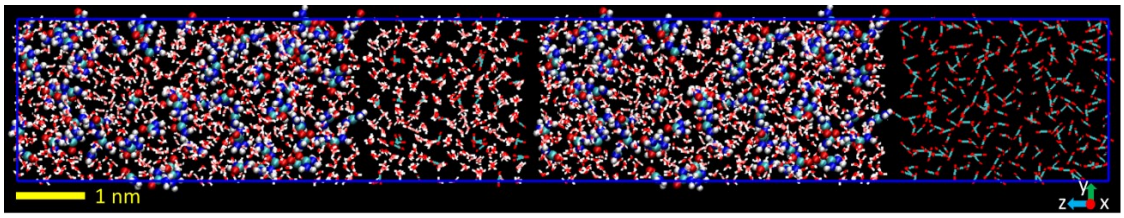

Figure S 4. The initial structure for simulating melting temperature and growth rate of CO_2 hydrate with the urea in the aqueous phase.

Table S 4. The solubility of urea in water at 1 bar and 298 K using different values of $\chi_{urea\text{-}water}$

$\chi_{urea\text{-}water}$	1.0	1.1	1.2	Exp [15]
solubility from dissolving (mol frac.)	0.142	0.252	> 0.297	0.263
solubility from growing (mol frac.)	0.146	0.295		

Table S 5. The heat of dissolution of urea in water at 1 bar and 298 K using different values of $\chi_{urea\text{-}water}$

$\chi_{urea\text{-}water}$	1.0	1.1	1.2	Exp [19]
heat of dissolution (X_{urea}=0.1) (kJ/mol)	18.2	16.8	14.8	14.4

Table S 6. The change (decrease) in CO_2 hydrate melting temperature in urea solution (X_{urea} = 0.1) at 45 bar. The melting temperature without urea is given in Table S 2.

$\chi_{urea\text{-}water}$	1.0	1.1	Exp [20]
melting temperature depression (K)	4	6	7

4. Hydrate Structural Characteristics Determination

The four-body order parameter (F4) order parameter was used to determine the structural characteristic of water molecules [21]. The F4 order parameter is defined as

$$F4 = \cos(3\theta) \qquad \text{(S1)}$$

where θ is the H-O ..... O-H dihedral angle of oxygen and outer-most hydrogens of the water dimer within 3.5Å (see Figure S 5 (a)). To reduce noise and enhance the contrast between liquid water and hydrate water, the following averaging was performed. First, the atomic coordinate was block averaged for 4 ps with 1 ps interval (i.e., using 4 frames). A raw F4 value of each water molecule was determined using the block averaged coordinates. The F4 value to be used in the subsequent analysis was averaged from 10 consecutive raw F4 values, i.e., averaged over 40 ps. The F4 value thus determined was 0 for liquid water molecules and 0.85 for water in the perfect hydrate lattice. We consider hydrate-like water to have an F4 value greater than 0.5.

The hydrate - liquid (solid–liquid) interfacial water molecules are identified as follows. A water molecule is considered to be at the interface if (1) its F4 value is between 0.3 to 0.7, and (2) at least two of its neighboring water molecules (within a spherical radius of 3.5 Å) have F4 greater than 0.5, and (3) at least two of its neighboring water molecules have F4 less than 0.5. (The interfacial water molecules are highlighted as red spheres in Figure S 6 (a)). The hydrate - liquid water interface is defined from the average of those identified interfacial water molecules (as indicated by the green dashed line in Figure S 6).

The mutually coordinated guest (MCG) order parameter [22] was used to identify CO_2 molecules being encapsulated in the hydrate cages. Any two CO_2 molecules within a separation distance of 9 Å are a candidate guest pair (illustrated in Figure S 5(b)). If there are at least 5 water molecules present within 6 Å to both of the pair guest molecules and lying within an intersection of the 90^O cones projected bidirectionally between the two guest molecules (yellow region in Figure S 5 (b)), then add to the "count" (N_c) to each of the candidate guest molecules. The N_c value of a CO_2 molecule is the sum of contributions from all the candidate pairs involving this CO_2 molecule. Similar to the F4 calculation, averaging of atomic coordinates (using 4 frames separated by 1 ps) and 10 N_c values from consecutive times are averaged for the final N_c value of each CO_2 molecule. Comparing the N_c distribution (Figure S 6 (c)) and F4 distribution

(Figure S 6 (b)), the CO_2 molecule is considered to be encapsulated in the hydrate if $N_c \geq 5$. For a perfect sI hydrate the N_c value of a gas molecule is around 12.

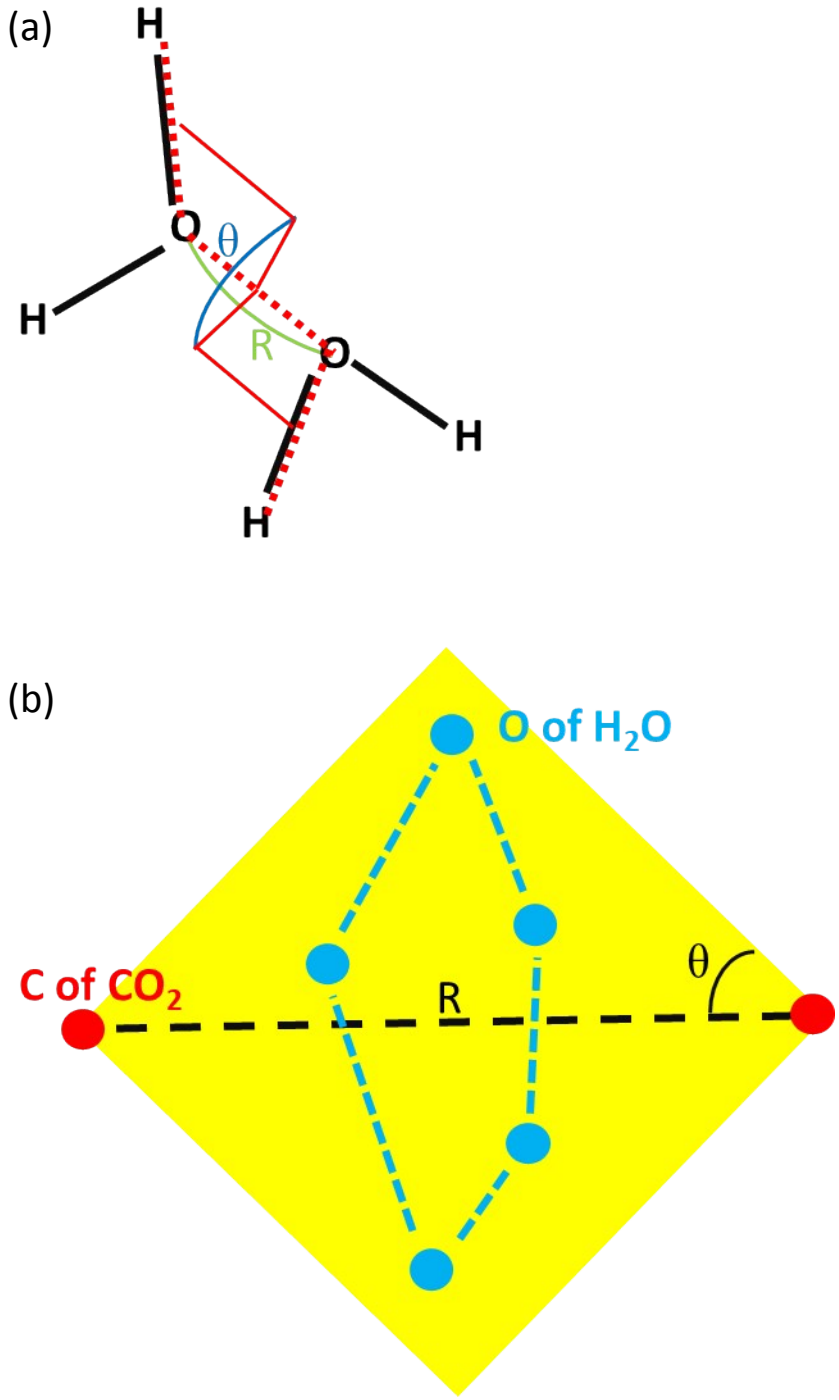

Figure S 5. (a) Illustration of the dihedral torsion θ and water separation R in F4 calculation where R < 3.5 Å. (b) Illustration of the angle θ and water separation R in MCG calculation where $\theta = 45^{O}$ and R < 9 Å.

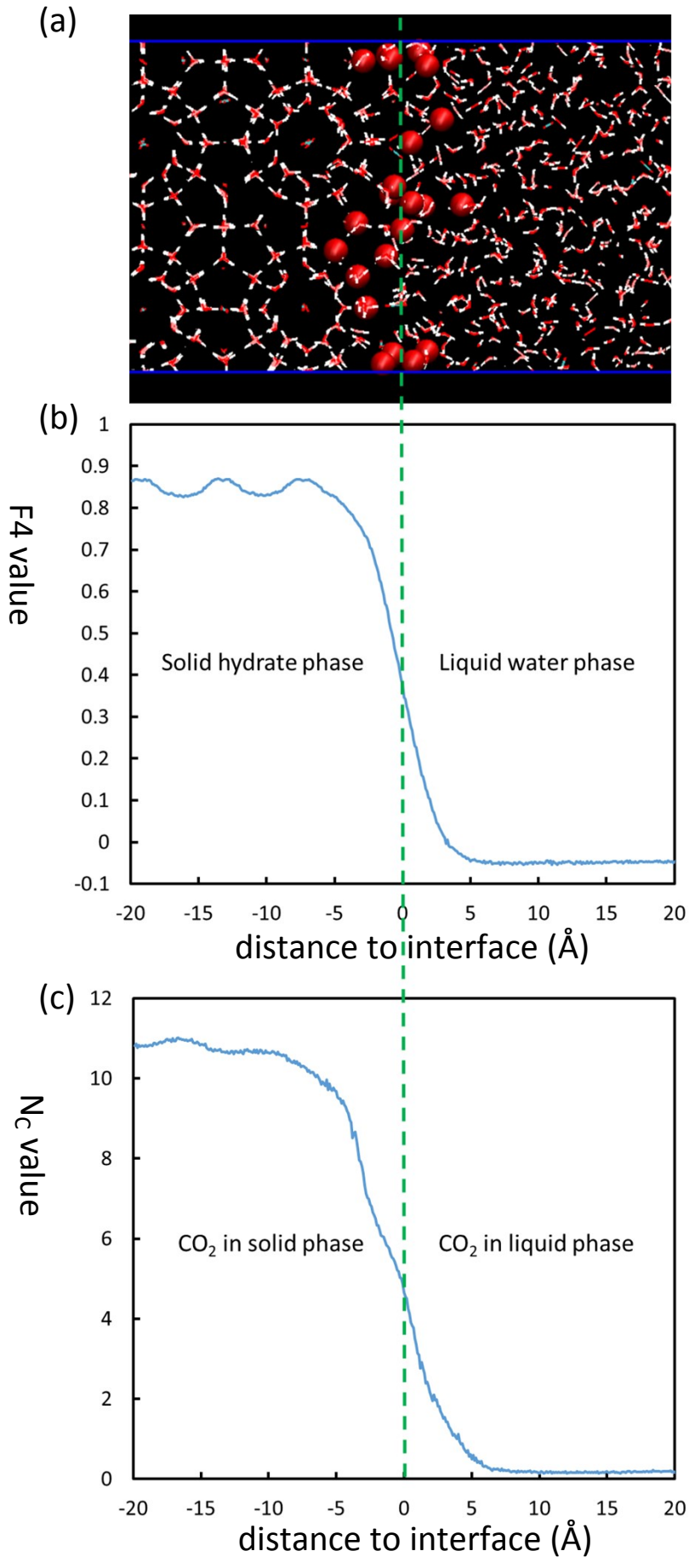
(a)
(b)
F4 value
Solid hydrate phase
Liquid water phase
distance to interface (Å)
(c)
N_C value
CO_2 in solid phase
CO_2 in liquid phase
distance to interface (Å)

Figure S 6. The solid–liquid interface (green dashed line) illustrated by the interfacial water molecules (the red spheres) (a), the distribution of F4 value of water molecules (b), and the distribution of N_c value of CO_2 molecules (c).

5. Melting point of CO_2 hydrates

The melting temperature under a pressure of 45 bar is determined using a series of NPT simulations at different temperatures: 278 K to 290 K for the system without urea, and 282 K to 286 K for the system with urea present. The time evolution of the system potential energy is shown in Figure S 7. The potential energy increases with time if the temperature is above its melting point (indicating melting of hydrate), while the potential energy decreases with time when the temperature is below the melting point (indicating growing of hydrate). When the potential energy fluctuates around the same value, the temperature is regarded as the melting point. Based on the results, the melting point of CO_2 hydrate is determined to be 285 K at 45 bar and the melting temperature drops to 283 K when urea is present (with a mole fraction of X_{urea} = 0.03). The thermodynamic inhibiting effect of urea is reproduced in our simulation, while the absolute melting temperatures are about 2 K higher than experiment data [13, 20].

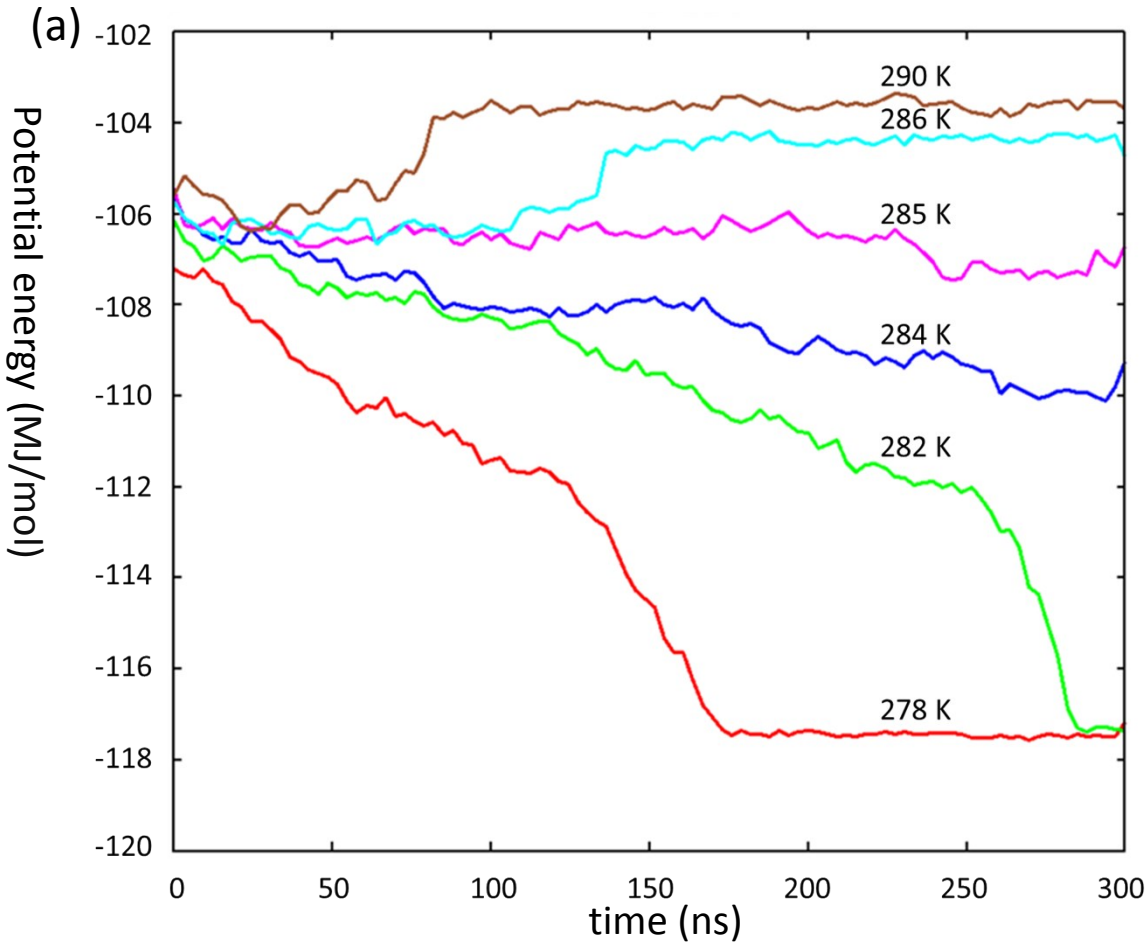

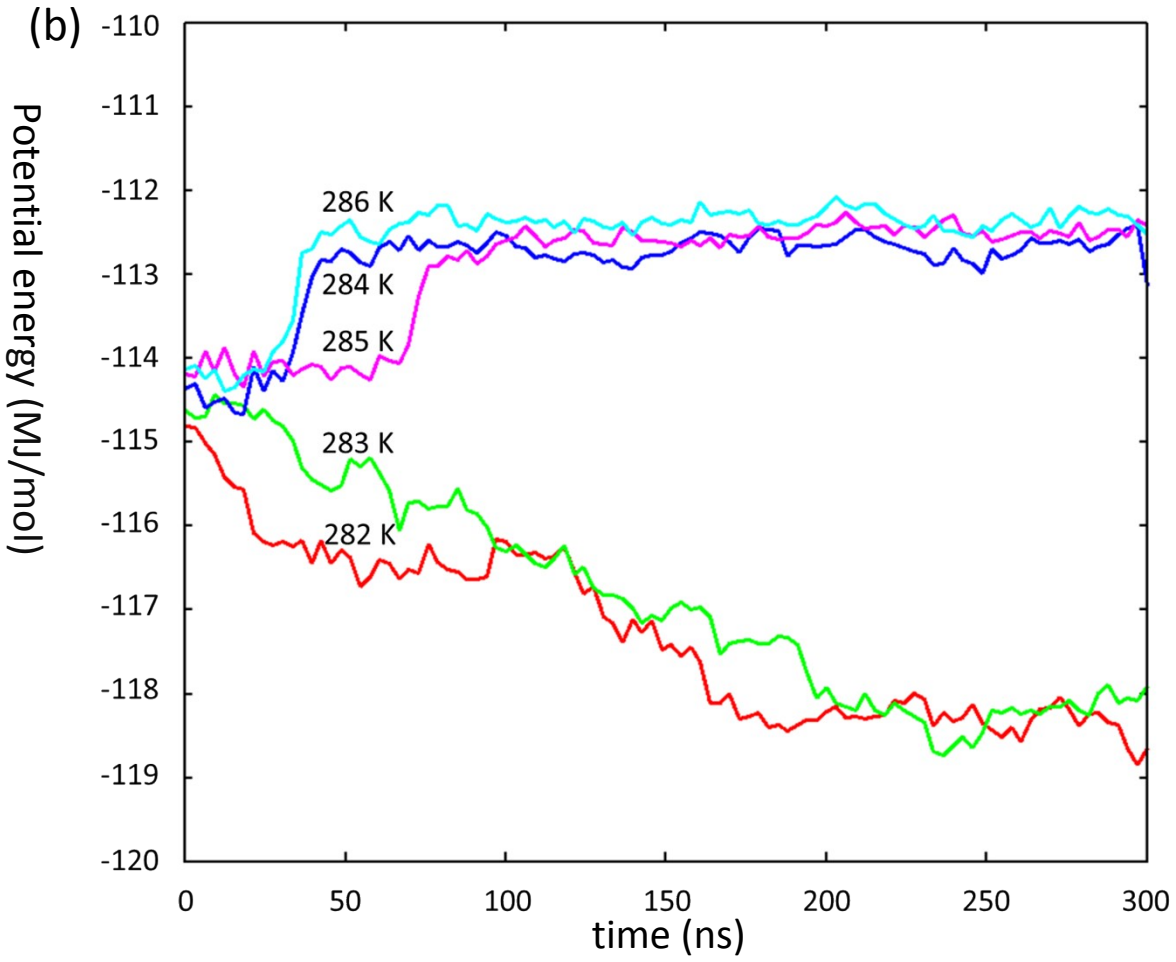

Figure S 7. The time evolution of potential energy from the three-phase CO_2 hydrate model at 45 bar and different temperatures without urea (a) and with urea present in the liquid phase (X_{urea} = 0.03) (b).

Table S 7. Comparison of the melting temperature of CO_2 hydrate at 45 bar from MD simulations and experiment

liquid phase	Tm from this study (K)	Tm from experiment (K)
pure water	285±1	283 [13]
X_{urea} = 0.03	283±1	281[a] [20]

[a]Estimate from experimental value of pressures from 16 bar to 33 bar.

6. Hydrate growth simulations

For the hydrate growth simulations, the time evolution of the amount of hydrate – like water is shown in Figure S 8 to Figure S 11. The plots of CO_2 solubility with time for the corresponding systems are shown from Figure S 12 to Figure S 14. The number of hydrate-like water remains nearly constant for the initial 30 ns. During this time period, the CO_2 molecules are dissolving to the liquid phase to approach equilibrium

solubility. The CO_2 dissolution process became steady after 30 ns. As the growth reaches a steady state, the increase of hydrate-like water becomes steady. Near the end of simulation (after 200 ns) the amount of hydrate–like water molecules increases rapidly because the liquid and gas phases became very thin and the dissolution of gas occurred rapidly. Note that for the urea containing system, urea concentration increases during the growth process, resulting in lowered melting temperature of hydrate (urea is a thermodynamic inhibitor). Therefore, the sub-cooling temperature continuous to drop as the growth process proceeds, resulting in the reduced growth rate after about 180 ns. The rapid rise of CO_2 concentration after 200 ns is due to mixing of gas phase and liquid phase or the whole system became hydrate caused the unusual solubility in the end of the simulation.

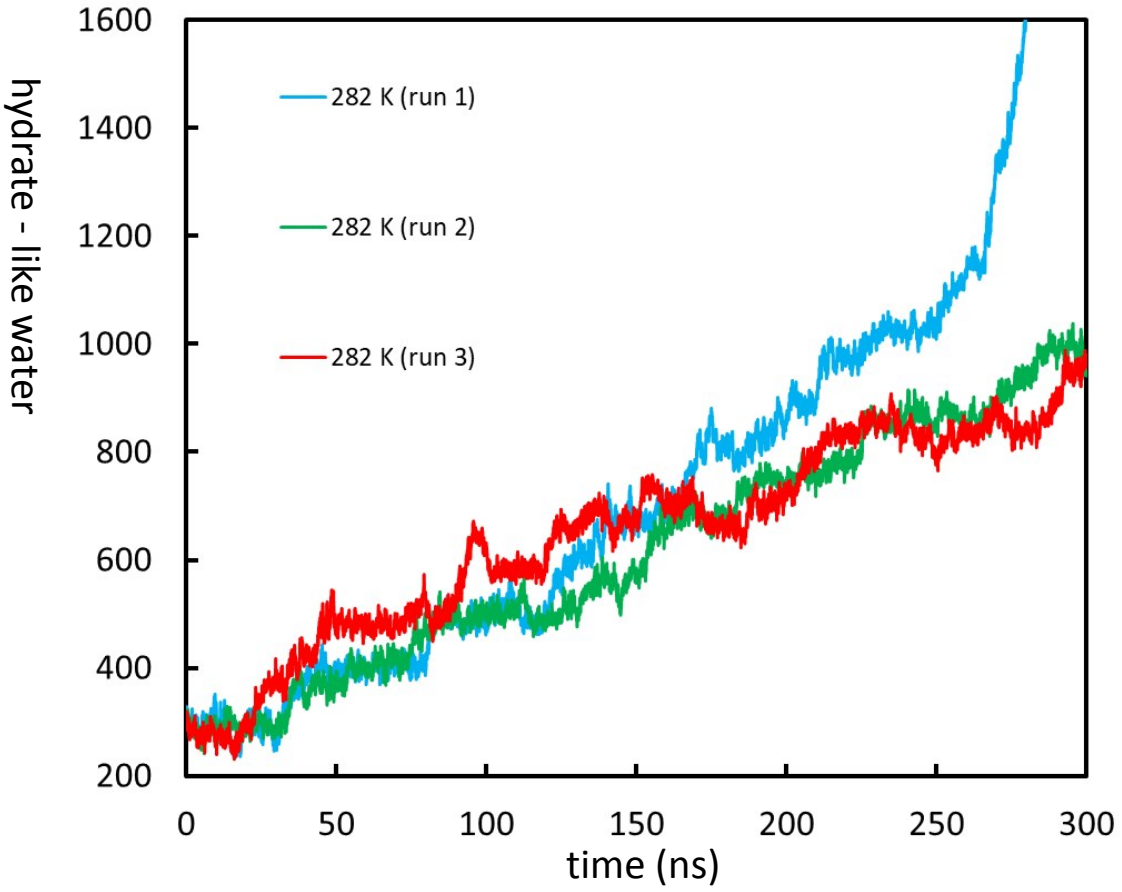

Figure S 8. The time evolution of the amount of hydrate–like water from the CO2 hydrate growth simulations at 282 K (without urea).

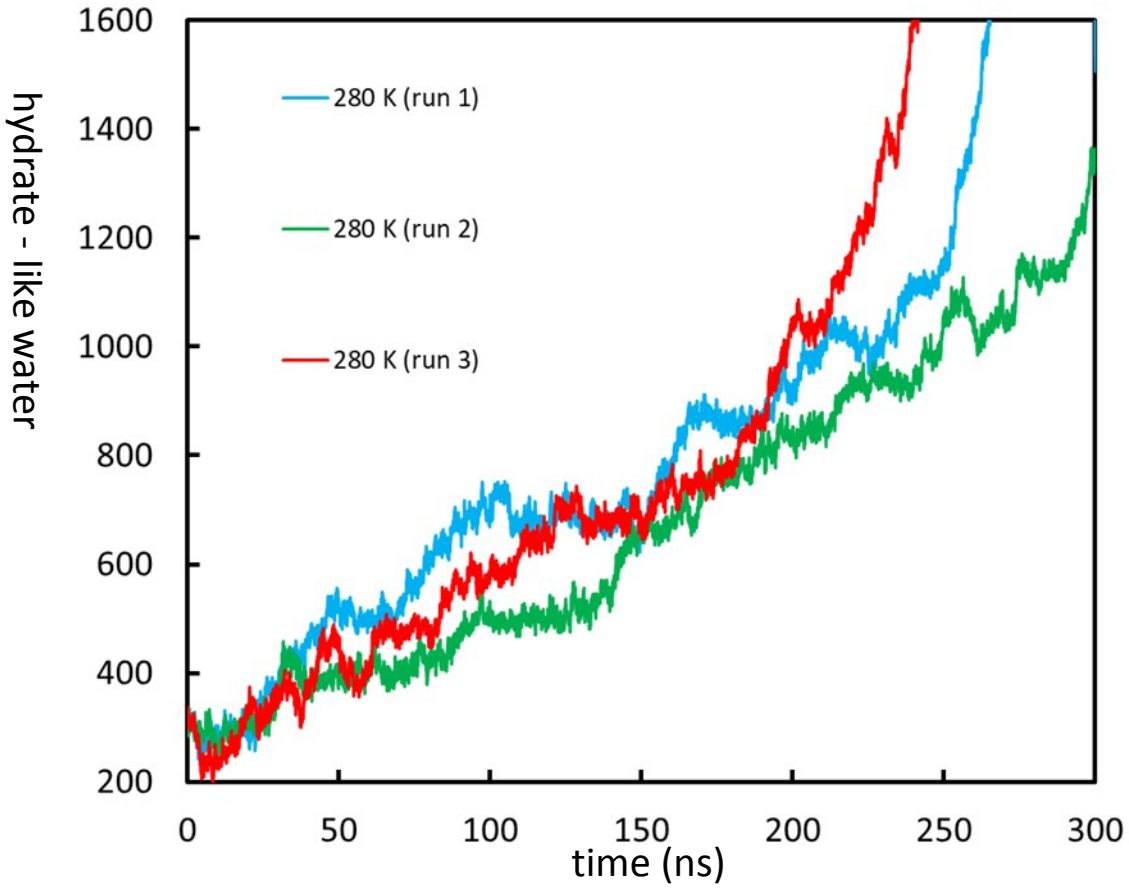

Figure S 9. The time evolution of the amount of hydrate–like water from the CO2 hydrate growth simulations at 280 K (without urea).

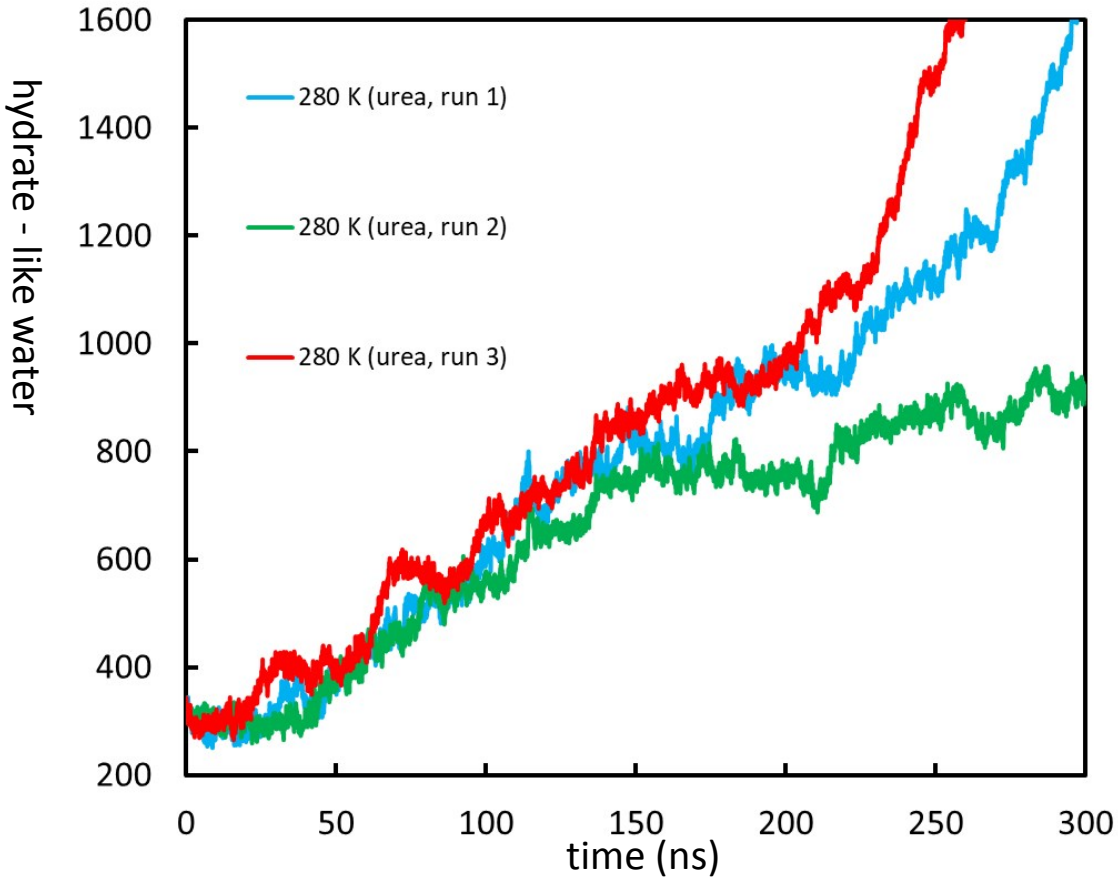

Figure S 10. The time evolution of the amount of hydrate–like water from the CO2 hydrate growth simulations at 280 K (with urea).

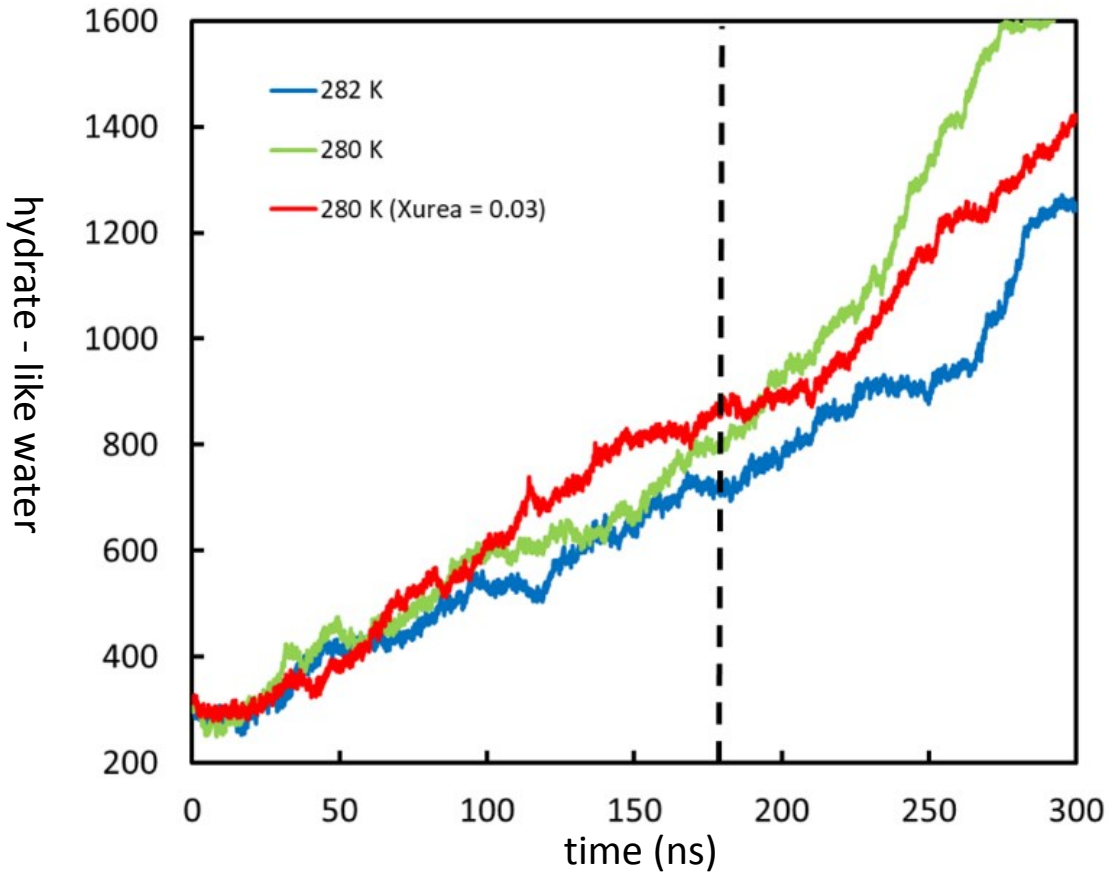

Figure S 11. Time evolution of total number of hydrate–like water in the hydrate growth simulations. Each line is an average of 3 independent runs.

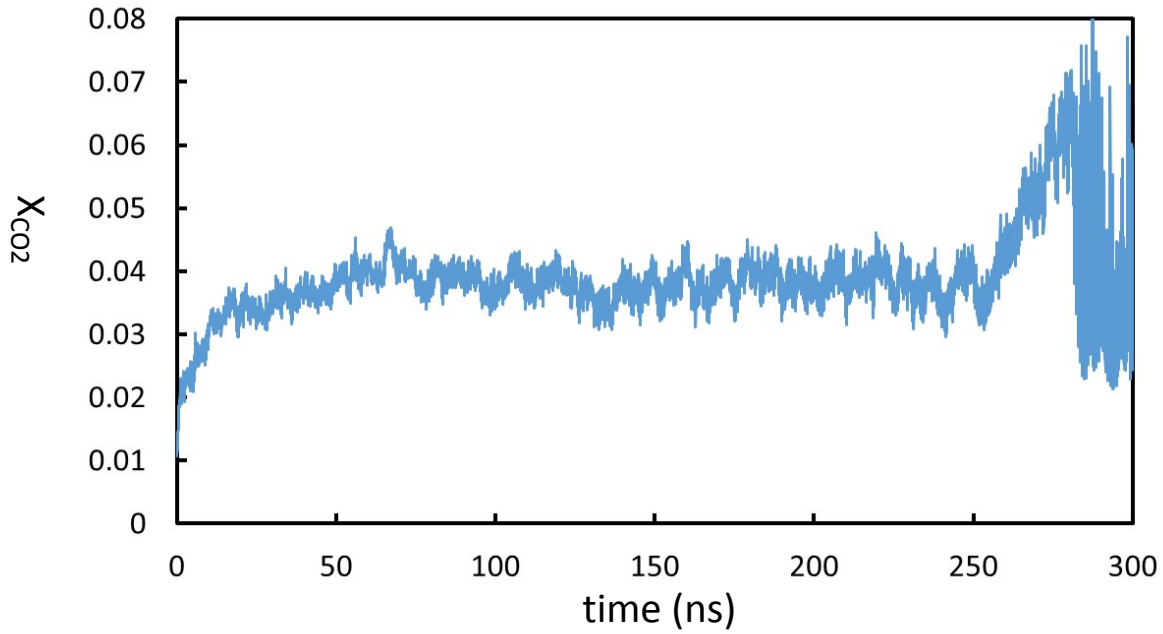

Figure S 12. The time evolution of CO_2 solubility from CO2 hydrate growth simulation (without urea) at 282 K (an average of 3 runs).

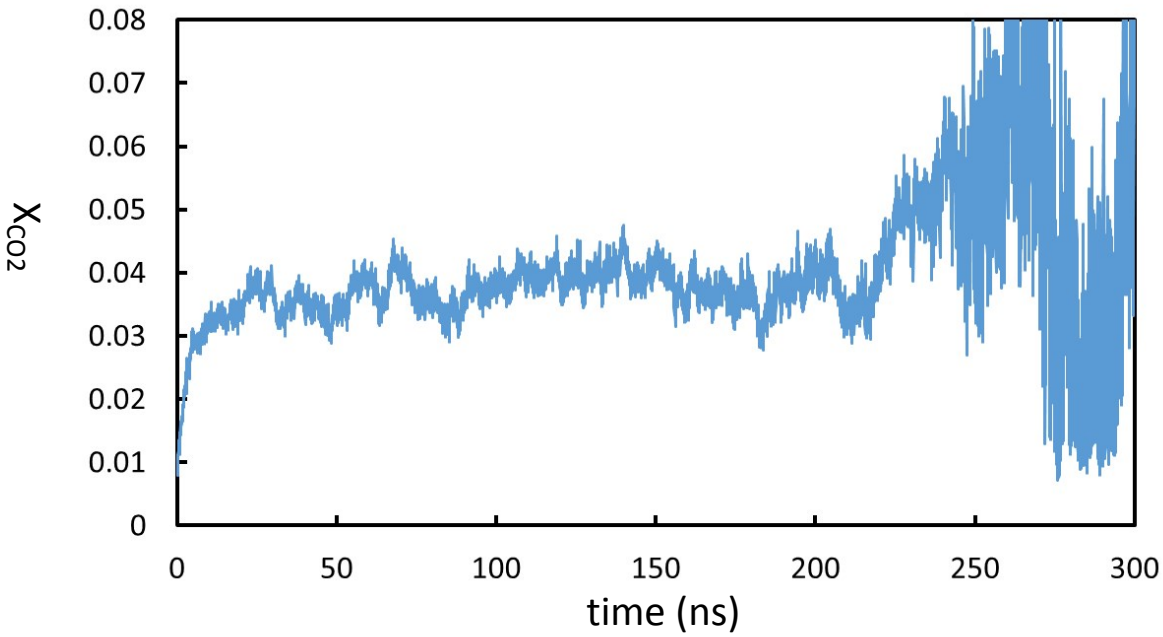

Figure S 13. The time evolution of CO_2 solubility from CO2 hydrate growth simulation (without urea) at 280 K (an average of 3 runs).

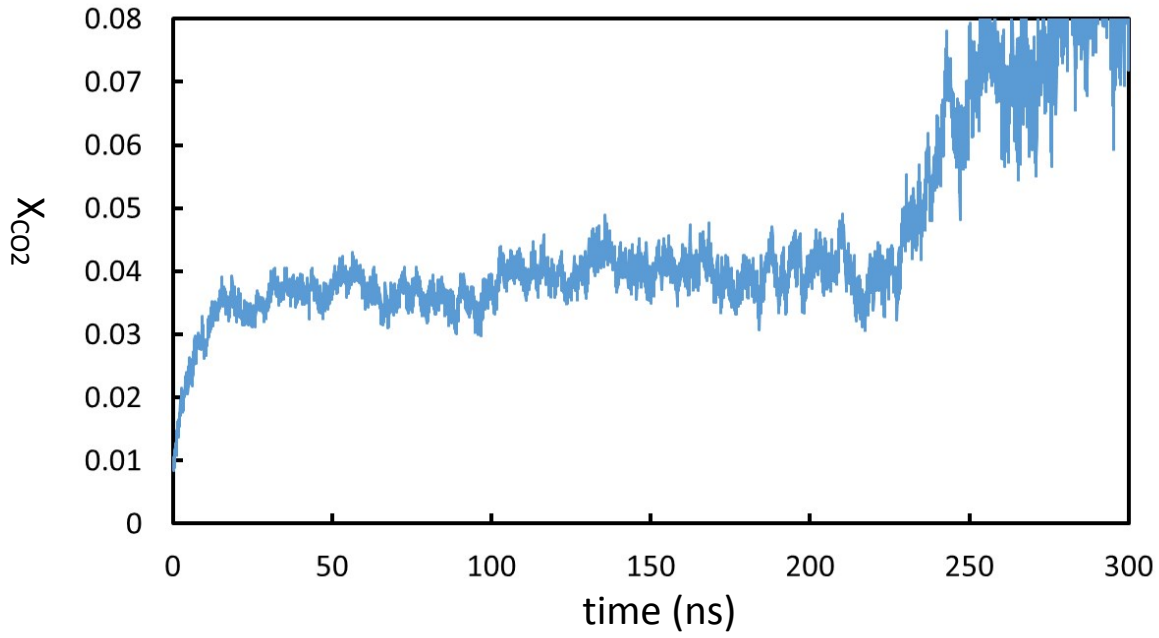

Figure S 14. The time evolution of CO_2 solubility from CO2 hydrate growth simulation (with urea) at 280 K (an average of 3 runs).

7. Concentration distribution and hydrate growth from each independent simulation

In the main text, we reported lowered peak intensity of the CO_2 concentration in the hydrate phase with the presence of urea (Figure 2). The same data from each individual simulation are shown in Figure S 15 to Figure S 32. In each simulation, the data were analyzed for each of the two solid-liquid interfaces (referred to as first and second solid-liquid interfaces in the figure captions). Note that a constant growth rate should give a flat CO_2 concentration despite of the layered CO_2 arrangement in hydrate phase. The fact that we do observe peaks and troughs in the hydrate phases ($x<0$), indicates that the hydrate layers grow in a stepwise manner. The reduced peak and trough intensity when urea is added indicates a faster and more continuous growth of the hydrate.

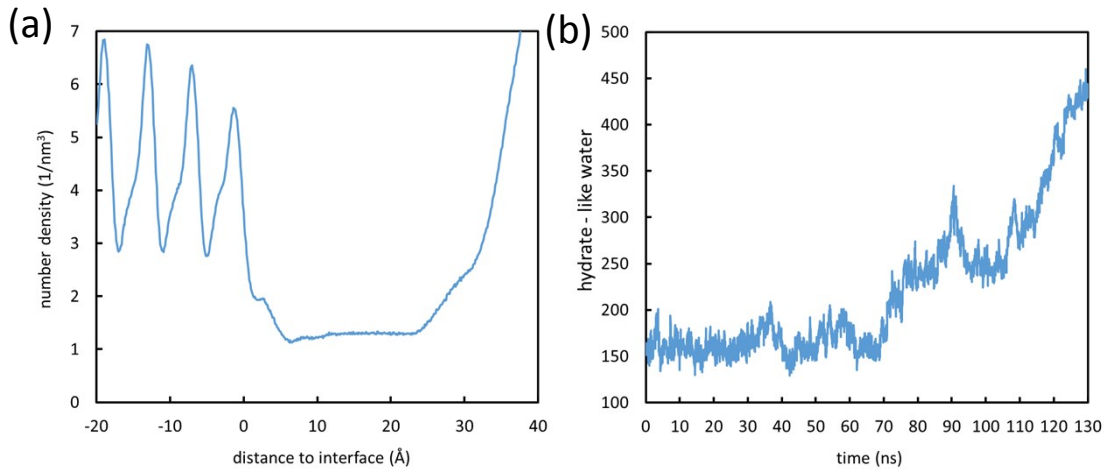

Figure S 15. The CO_2 concentration distribution (a) and time evolution of hydrate–like water (b) near the first solid–liquid interface of run 1 (282 K, without urea).

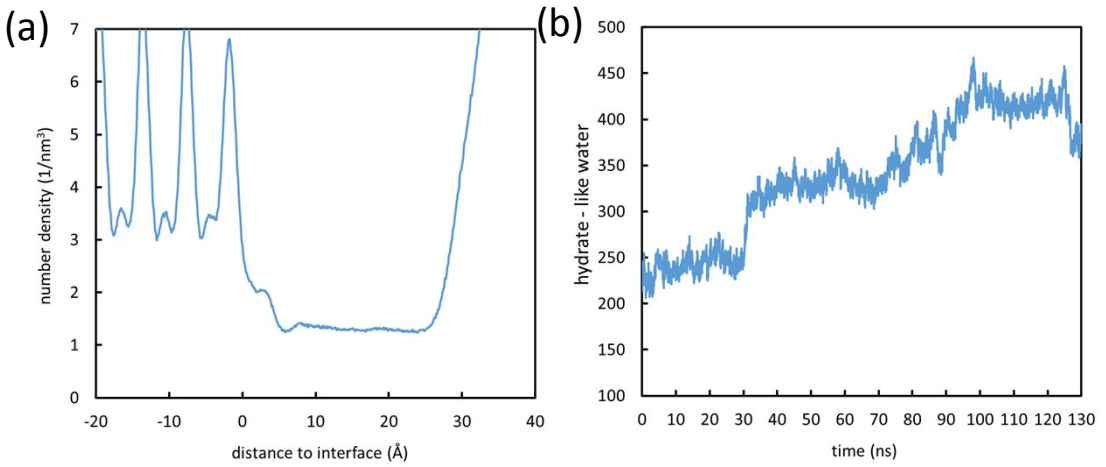

Figure S 16. The CO_2 concentration distribution (a) and time evolution of hydrate–like water (b) near the second solid–liquid interface of run 1 (282 K, without urea).

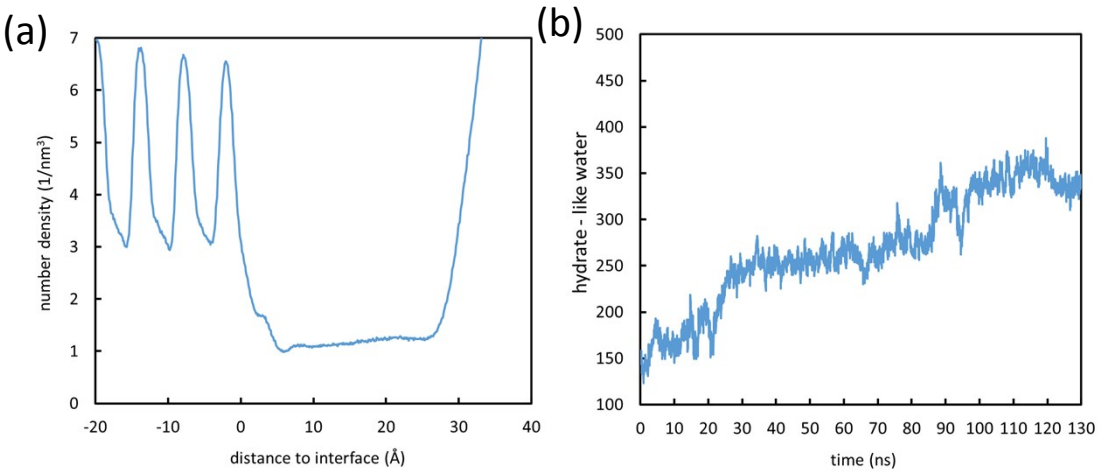

Figure S 17. The CO_2 concentration distribution (a) and time evolution of hydrate–like water (b) near the first solid–liquid interface of run 2 (282 K, without urea).

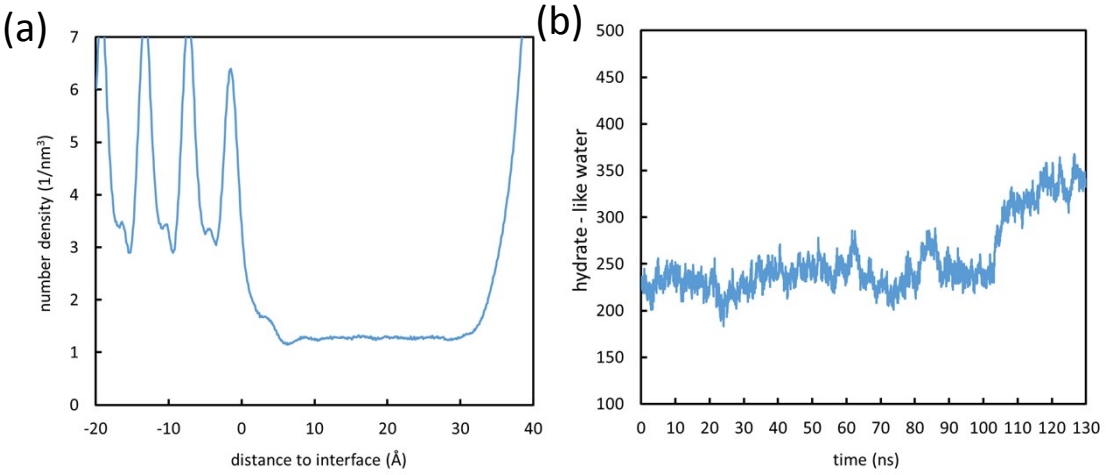

Figure S 18. The CO_2 concentration distribution (a) and time evolution of hydrate–like water (b) near the second solid–liquid interface of run 2 (282 K, without urea).

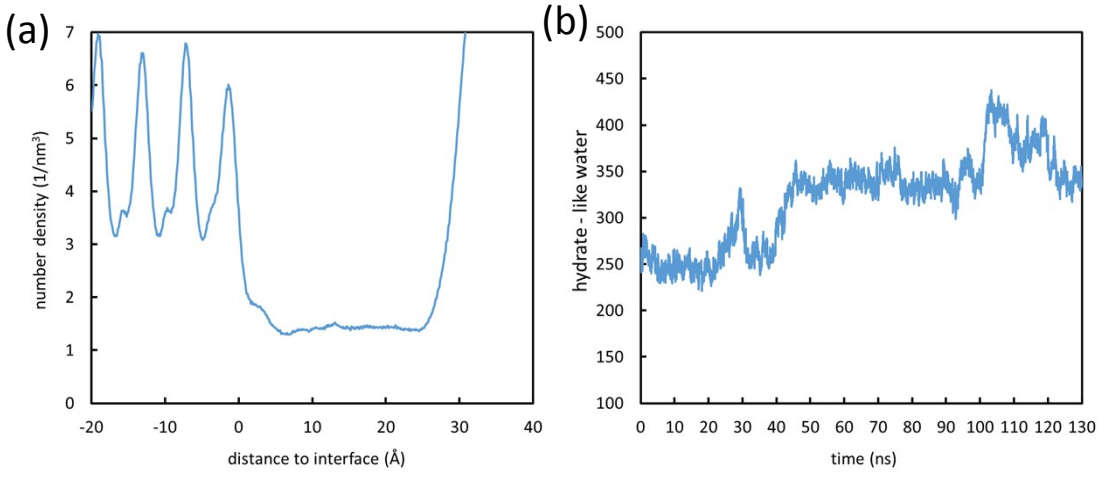

Figure S 19. The CO_2 concentration distribution (a) and time evolution of hydrate–like

water (b) near the first solid–liquid interface of run 3 (282 K, without urea).

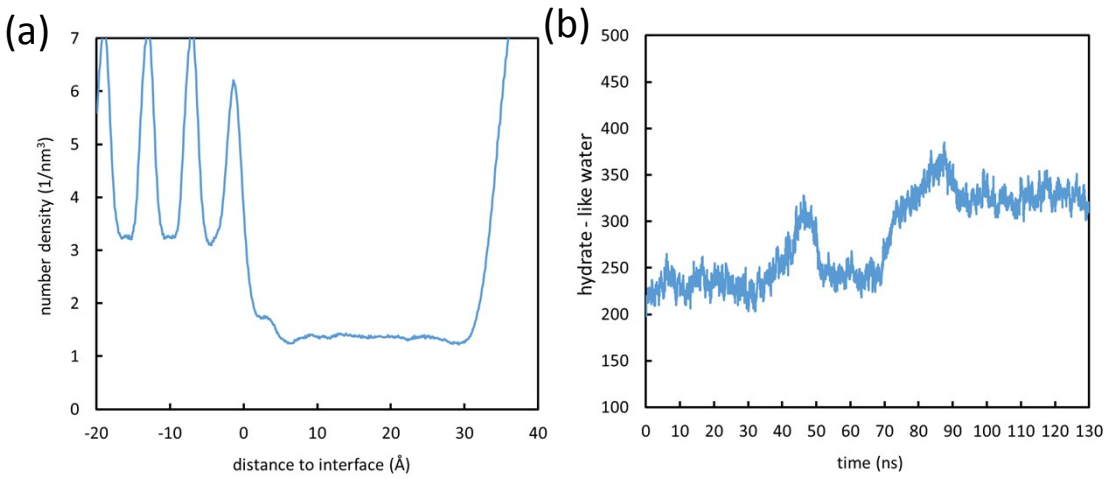

Figure S 20. The CO_2 concentration distribution (a) and time evolution of hydrate–like water (b) near the second solid–liquid interface of run 3 (282 K, without urea).

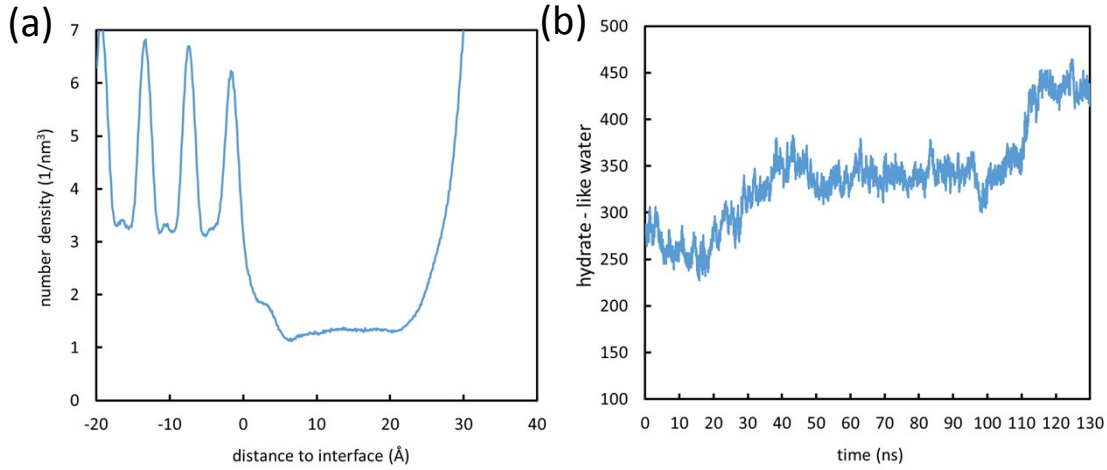

Figure S 21. The CO_2 concentration distribution (a) and time evolution of hydrate–like water (b) near the first solid–liquid interface of run 1 (280 K, without urea).

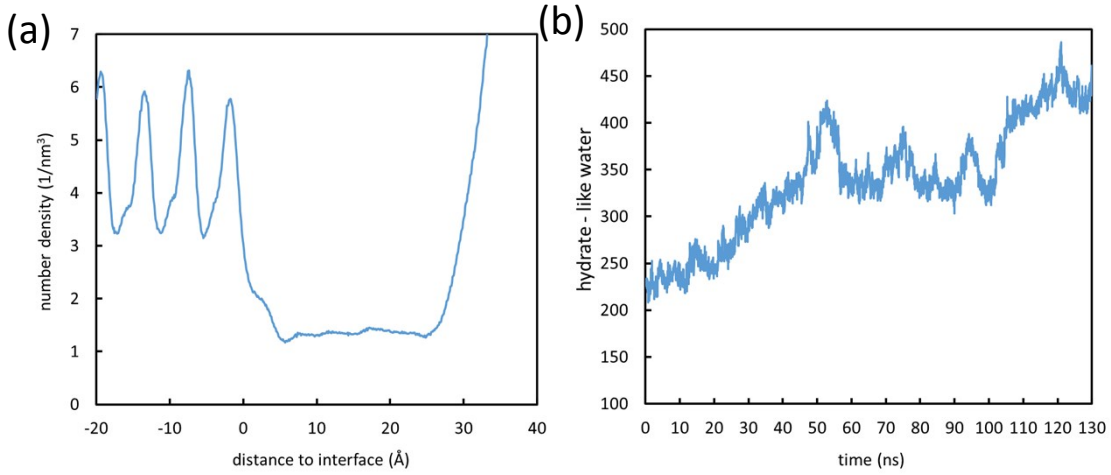

Figure S 22. The CO_2 concentration distribution (a) and time evolution of hydrate–like water (b) near the second solid–liquid interface of run 1 (280 K, without urea).

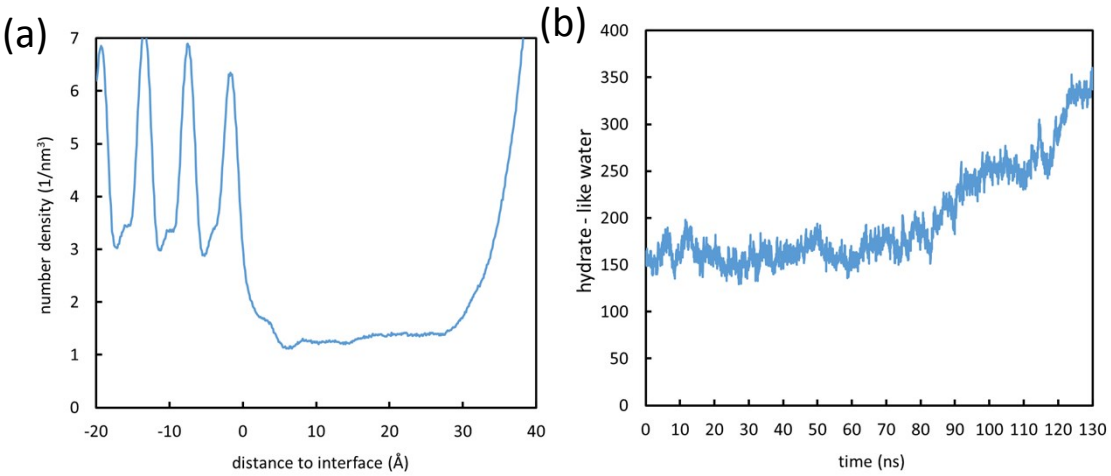

Figure S 23. The CO_2 concentration distribution (a) and time evolution of hydrate–like water (b) near the first solid–liquid interface of run 2 (280 K, without urea).

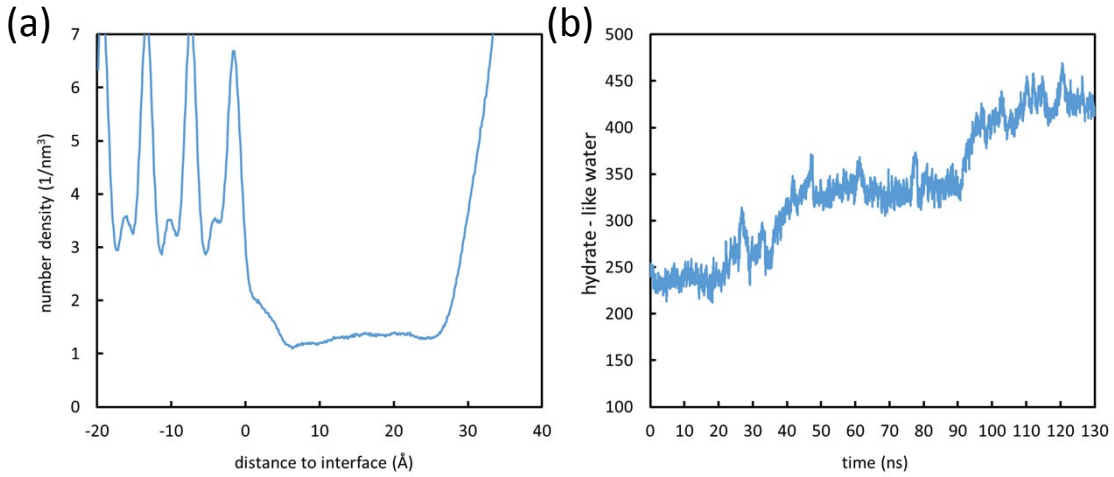

Figure S 24. The CO_2 concentration distribution (a) and time evolution of hydrate–like water (b) near the second solid–liquid interface of run 2 (280 K, without urea).

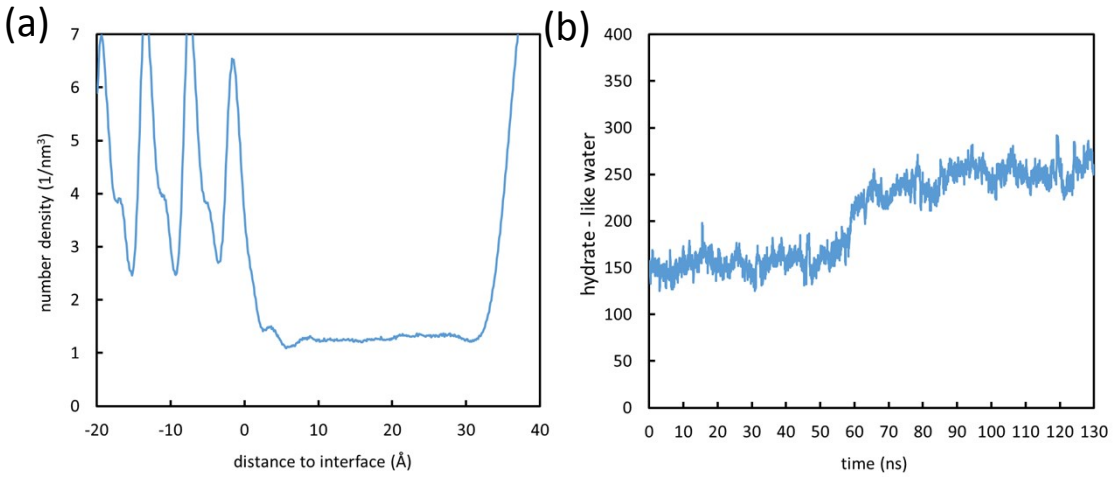

Figure S 25. The CO_2 concentration distribution (a) and time evolution of hydrate–like water (b) near the first solid–liquid interface of run 3 (280 K, without urea).

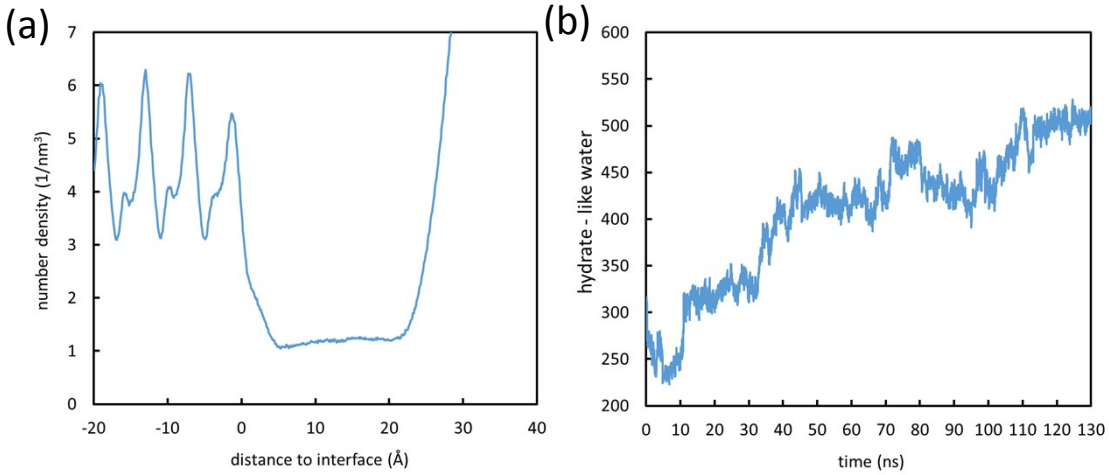

Figure S 26. The CO_2 concentration distribution (a) and time evolution of hydrate–like water (b) near the second solid–liquid interface of run 3 (280 K, without urea).

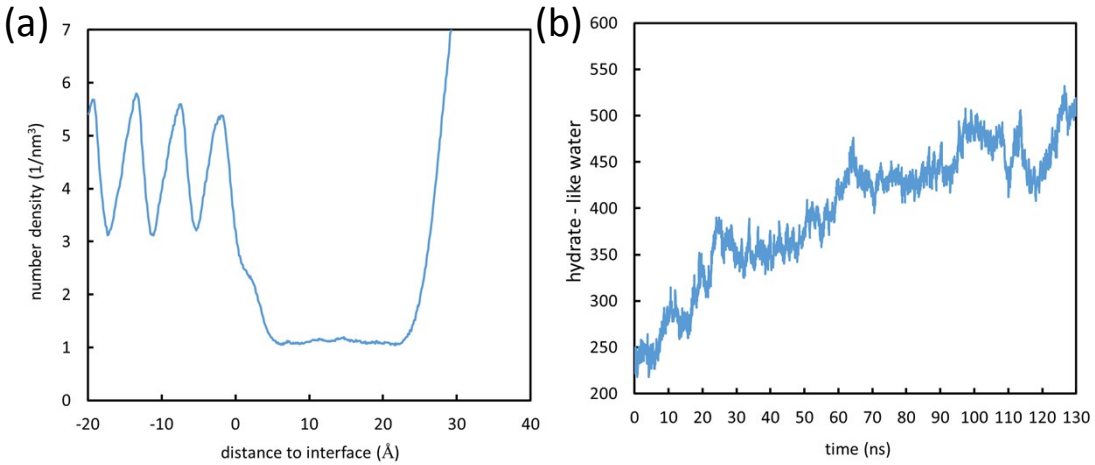

Figure S 27. The CO_2 concentration distribution (a) and time evolution of hydrate–like water (b) near the first solid–liquid interface of run 1 (280 K, with urea).

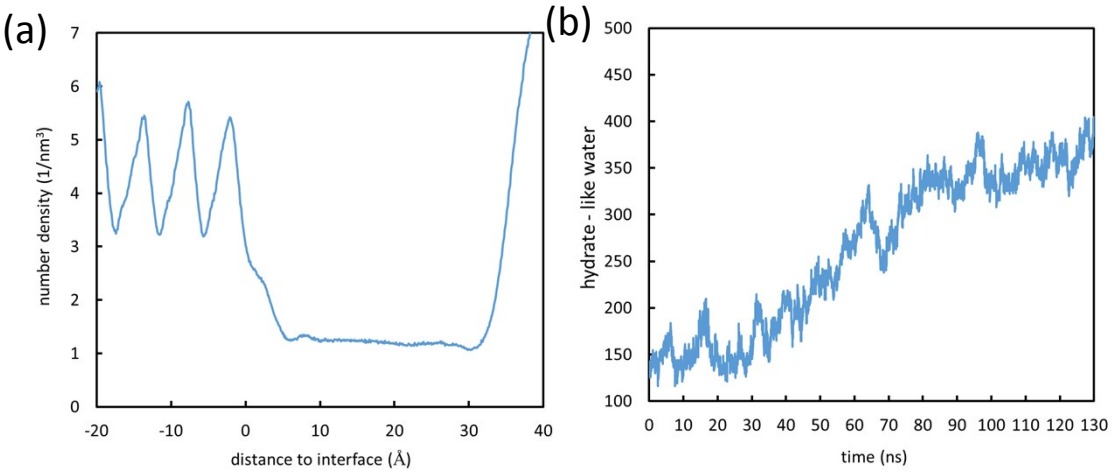

Figure S 28. The CO_2 concentration distribution (a) and time evolution of hydrate–like water (b) near the second solid–liquid interface of run 1 (280 K, with urea).

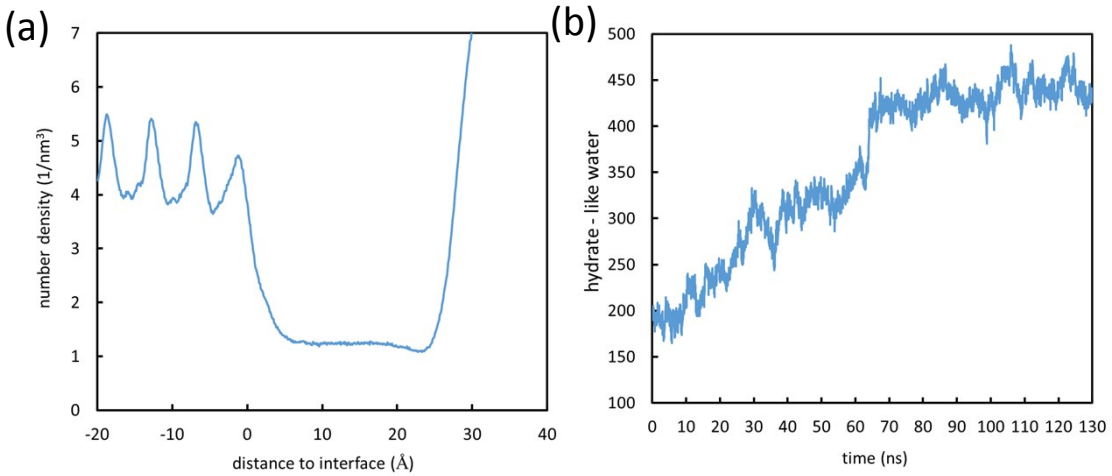

Figure S 29. The CO_2 concentration distribution (a) and time evolution of hydrate–like water (b) near the first solid–liquid interface of run 2 (280 K, with urea).

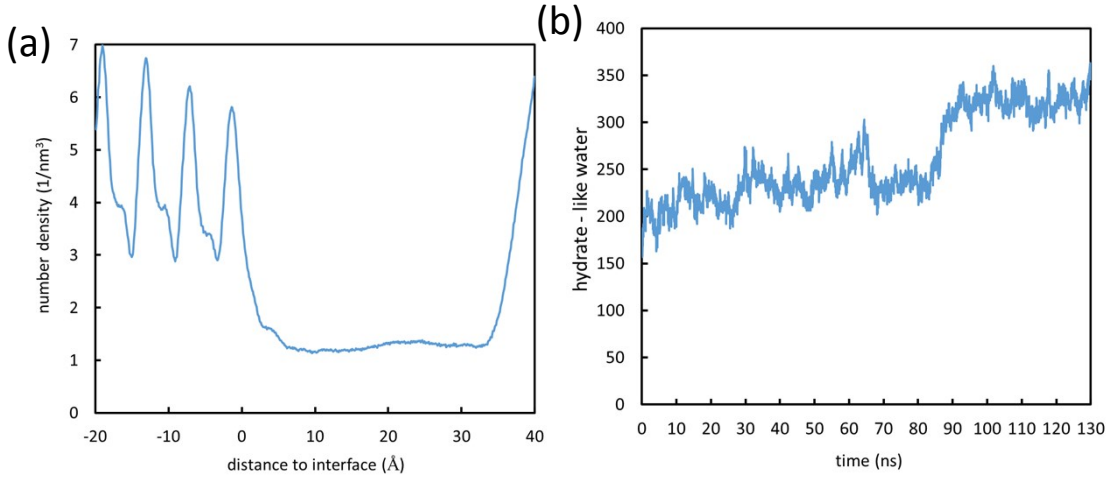

Figure S 30. The CO_2 concentration distribution (a) and time evolution of hydrate–like

water (b) near the second solid–liquid interface of run 2 (280 K, with urea).

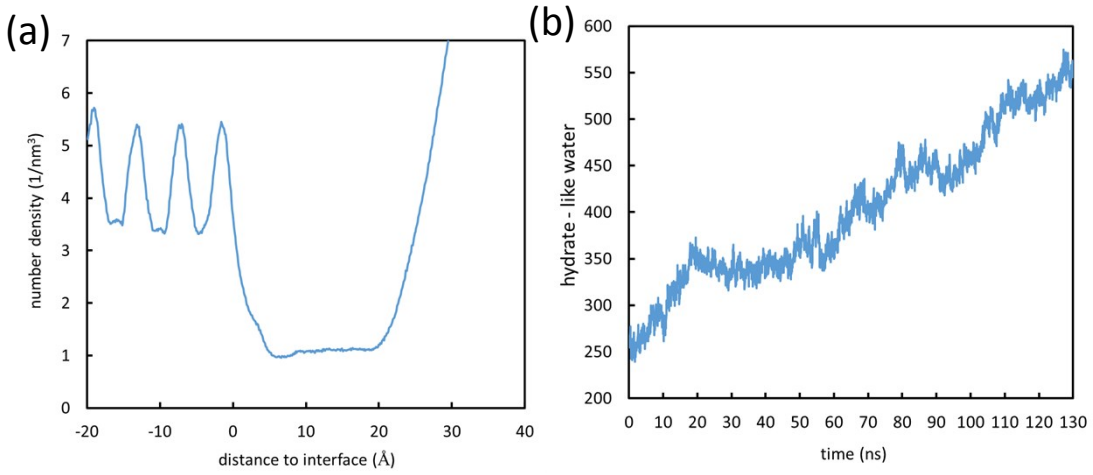

Figure S 31. The CO_2 concentration distribution (a) and time evolution of hydrate–like water (b) near the first solid–liquid interface of run 3 (280 K, with urea).

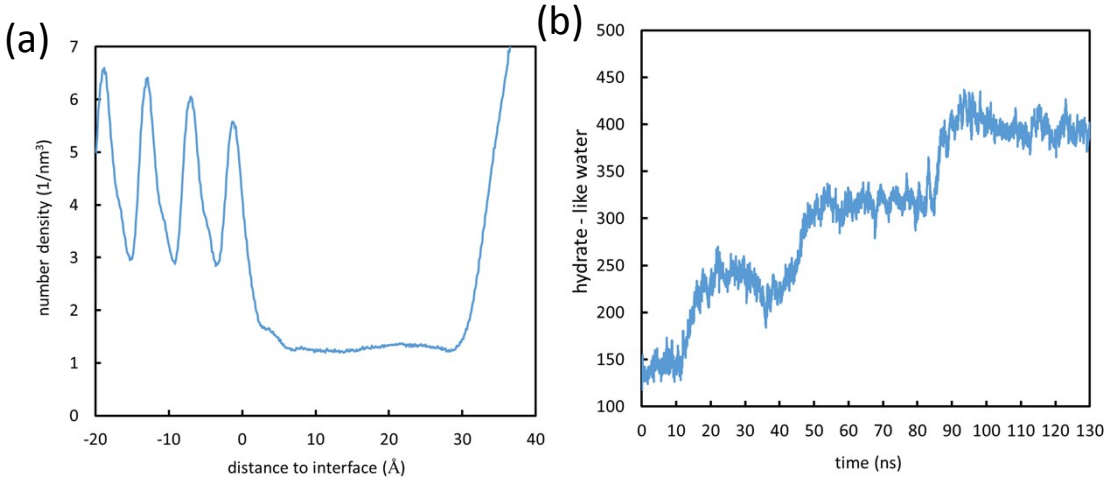

Figure S 32. The CO_2 concentration distribution (a) and time evolution of hydrate–like water (b) near the second solid–liquid interface of run 3 (280 K, with urea).

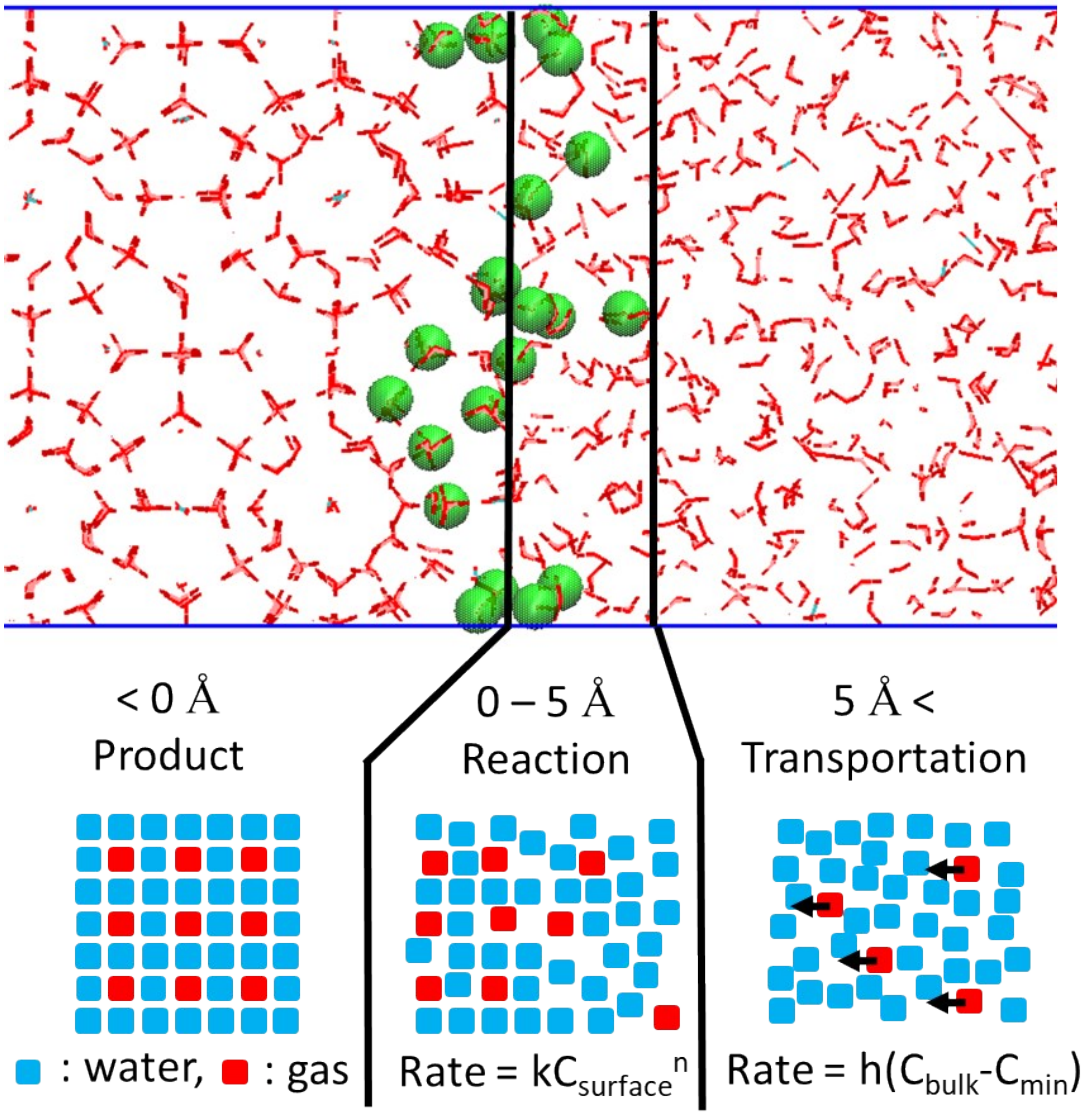

Figure S 33. Schematic diagram of the reaction–diffusion model.

8. Equilibrium data

For comparison, we also performed simulations around three-phase coexisting conditions. The results of CO_2 distribution near the solid-liquid interface are shown in Figure S 34 and Table S 8. The growth of hydrates without urea has a lower surface CO_2 concentration (1.95 CO_2/nm^3 for 282 K growth and 1.89 CO_2/nm^3 for 280 K growth vs. 2.06 CO_2/nm^3 for equilibrium) and a deeper concentration minimum (smaller C_{min}/C_{bulk}, 0.90 for 282 K growth and 0.86 for 280 K growth vs. 0.94 equilibrium). This again indicates that the growth rate is limited by the deficiency of CO_2 near the surface and slow mass transport of CO_2 from bulk to the interface.

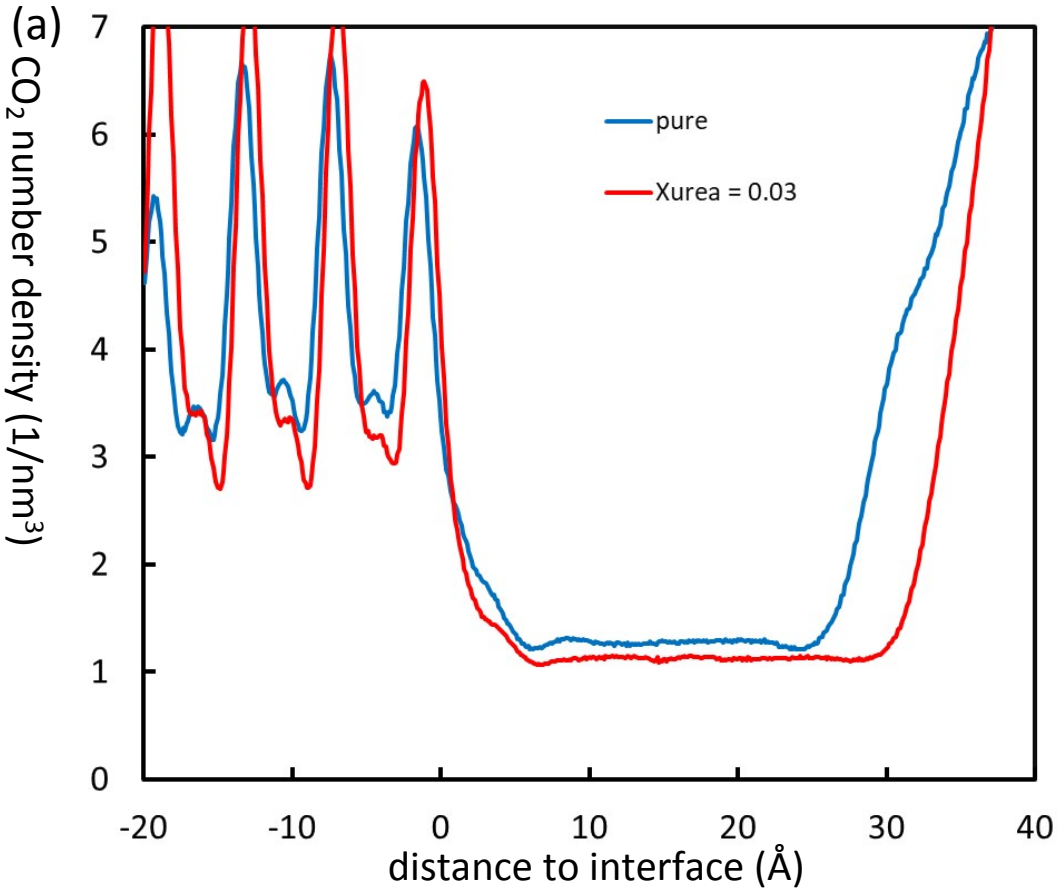
(a)
CO_2 number density ($1/nm^3$)
0
1
2
3
4
5
6
7
-20
-10
0
10
20
30
40
distance to interface (Å)
pure
Xurea = 0.03

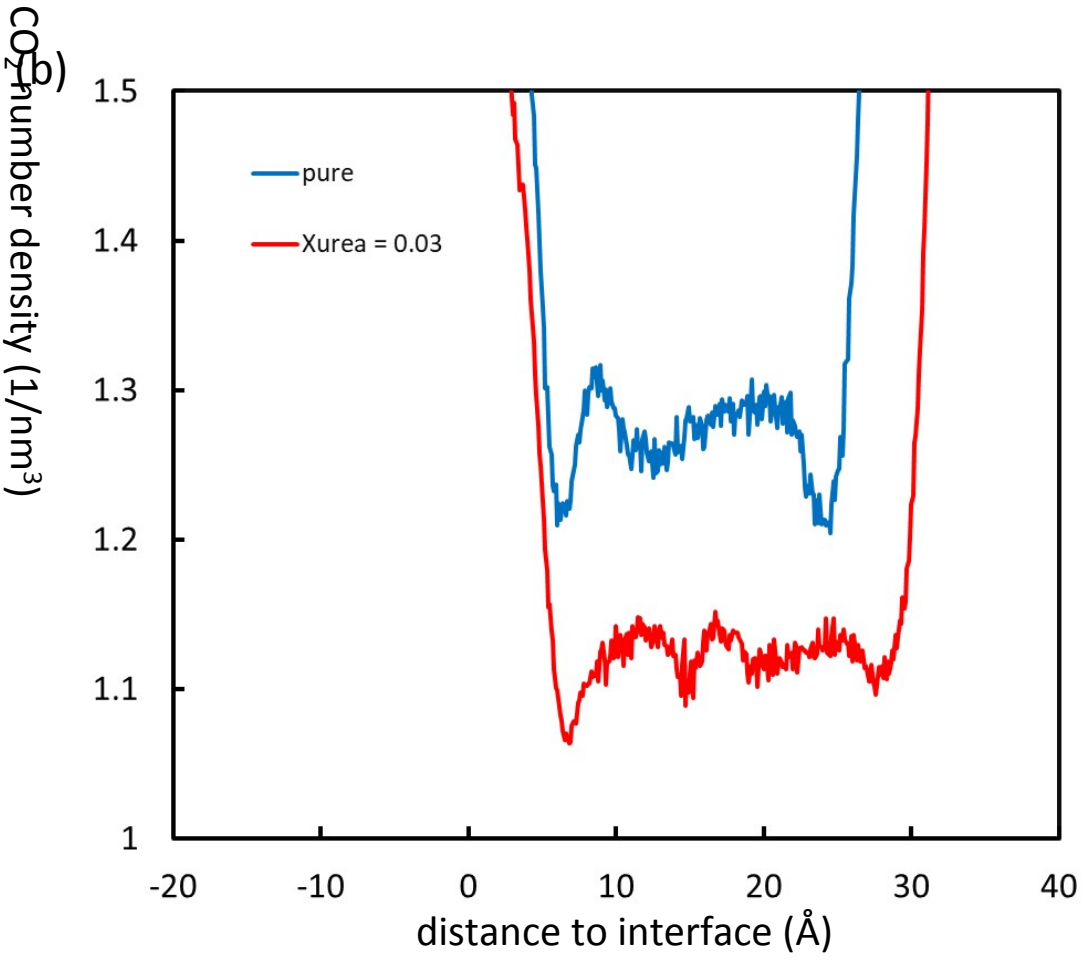

Figure S 34. The CO_2 concentration distribution (number density) near the solid-liquid interface of equilibrium systems (a). (b) is a zoom-in of figure (a) in the liquid phase to better show the concentration gradient. Each line is an average of 4 data (2 interfaces from 2 independent simulations).

Table S 8. Concentration data from equilibrium simulations. Each value is an average of 4 data (2 interfaces from 2 independent simulations).

condtion	$C_{surface}$ (standard error) ($1/nm^3$)	C_{bulk} (standard error) ($1/nm^3$)	C_{min} (standard error) ($1/nm^3$)	C_{min}/C_{bulk} (standard error)	X_{urea} (urea/(urea+water))
Pure water	2.060 (0.056)	1.267 (0.030)	1.192 (0.037)	0.941 (0.022)	0
X^{O}_{urea} = 0.03	1.938 (0.051)	1.128 (0.030)	1.049 (0.052)	0.928 (0.024)	0.035 (0.002)

9. Catalytic effect of urea on the hydrate formation

The distribution of F4 near the solid-liquid interface from hydrate growth simulations is shown in Figure S 35. For comparison, the distribution from equilibrium systems is shown in Figure S 36. The results show that the addition of urea can slightly increase the F4 value in the bulk phase and in the surface growing region (0 Å to 5 Å in front of the hydrate surface). The higher F4 value means that the water arrangement is more like that of hydrate.

The distribution of urea near the solid-liquid interface from hydrate growth simulations is shown in Figure S 37. The distribution from equilibrium simulations is shown in Figure S 38. The results show that urea molecules prefer to stay near the gas-liquid interface and do not have a particular affinity to the solid-liquid interface.

To understand how the presence of urea at the hydrate-water interface promotes the growth of CO_2 hydrates, we check if there is a preferred orientation of urea molecules at the interface based on the inclusion angle θ of the O=C vector and the surface normal (see **Figure S 39**) as Equation S2

$$\theta = \cos^{-1}\left(\frac{\vec{O=C} \bullet \vec{n_z}}{|\vec{O=C}||\vec{n_z}|}\right) \quad \text{(S2)}$$

The average angle distribution (from 6 surfaces of 3 independent simulations) of urea molecules along the solid-liquid interface from the growth simulations is shown in Figure S 40. In the bulk (10 Å < x < 20 Å) the average θ of about 1.57 (π/2) indicates no preferred orientation of urea in water. There is a clear reduction of the angle for surface urea molecules (0 Å < x < 5 Å), indicating that the oxygen atom of urea prefers to align slightly towards the solid phase. The data in the solid phase (x < 0 Å) is subjected to high statistical uncertainty because urea is rarely trapped in the solid phase.

The average θ distribution from equilibrium simulations is shown in Figure S 41. The results show O=C tends to point toward the hydrate surface when urea molecules are near the solid-liquid interface. O=C also tends to point toward the gas - liquid interface when urea molecules are near the gas-liquid interface.

The hydrate growth process will be hindered if the additives bind to the hydrate surface longer than the characteristic time of hydrate growth. This was also discussed in Yagasaki's work [23]. The residence time distribution of urea molecules within 5 Å in front of the hydrate surface is given in Figure S 42. The plot includes data from 6 solid–liquid interfaces of 3 sets of simulation. The residence time is the time duration of a urea molecule staying within 5 Å in front of the hydrate surface. The residence time is seldom longer than 5 ns, and the maximum residence time is less than 30 ns. The residence time of urea molecules around the hydrate surface (within 5 Å) is shorter than the characteristic time of hydrate growth (about 40 ns, i.e., it takes about 40 ns to grow 5 Å thick of hydrate). Thus, urea molecules do not block the hydrate growth. The

maximum residence time of urea molecules and growth rate of each solid-liquid interface is given in Table S 9. After examining several urea molecules that stayed on the surface for a long time, we found that urea can be trapped in an incomplete cage ($5^{12}6^2$). However, the urea molecule eventually leaves in order to form a complete cage. An example is shown as Figure S 43.

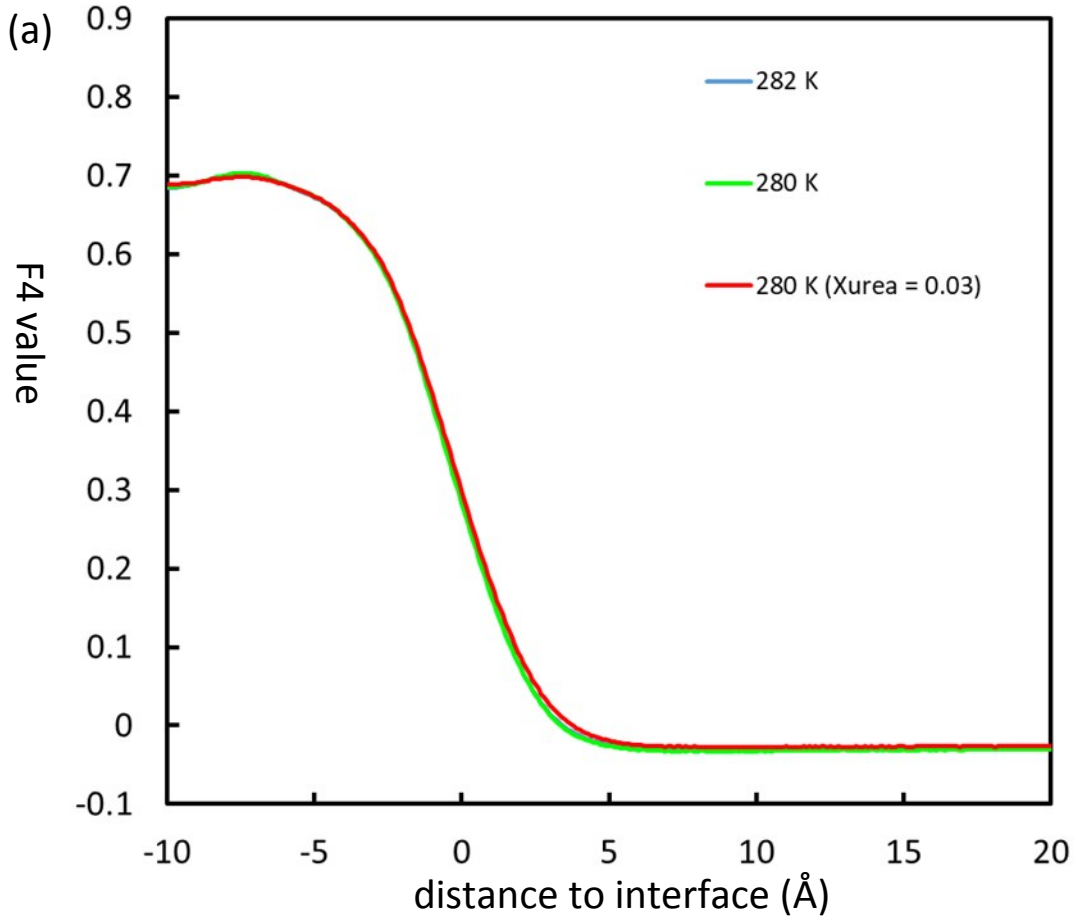

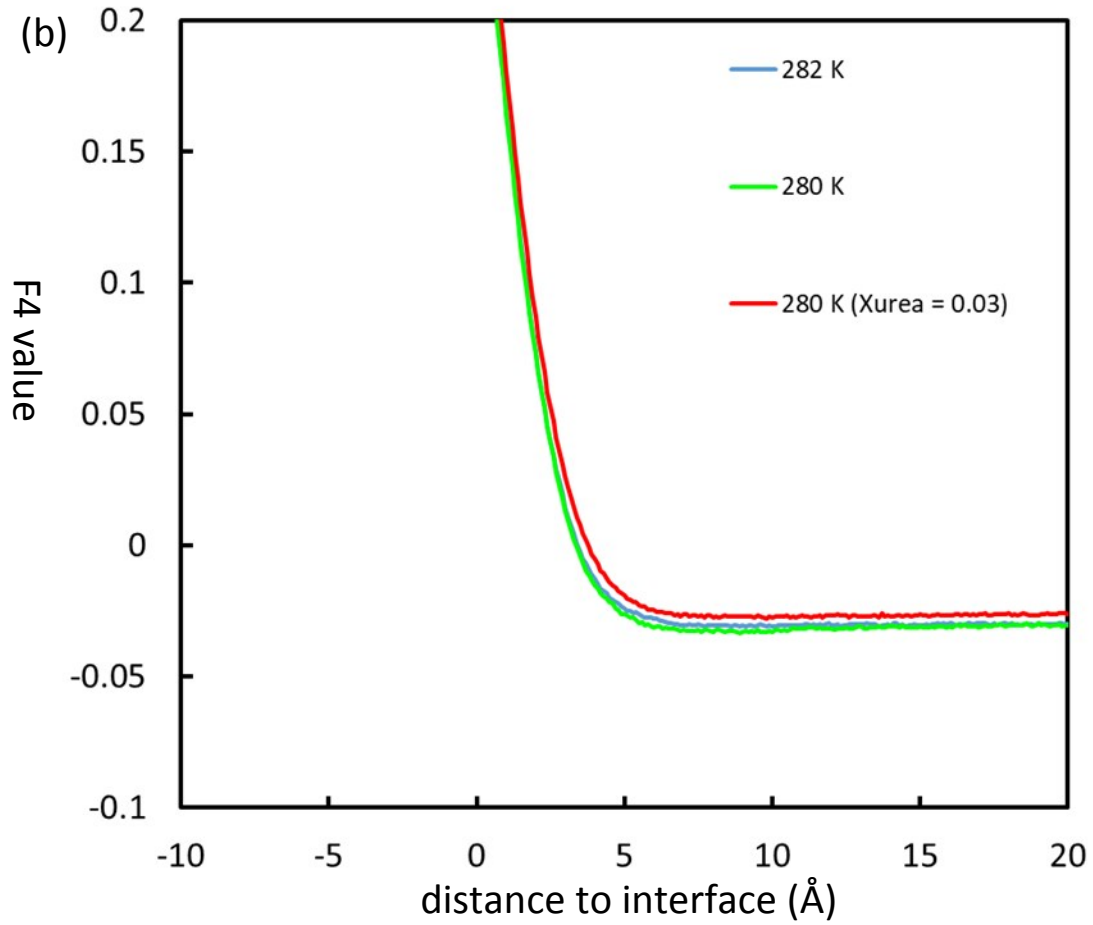

Figure S 35. The F4 distribution near the solid-liquid interface from hydrate growth simulations (a). (b) Zoom in of the interface. Each line is an average of 6 data (2 interfaces from 3 independent simulations).

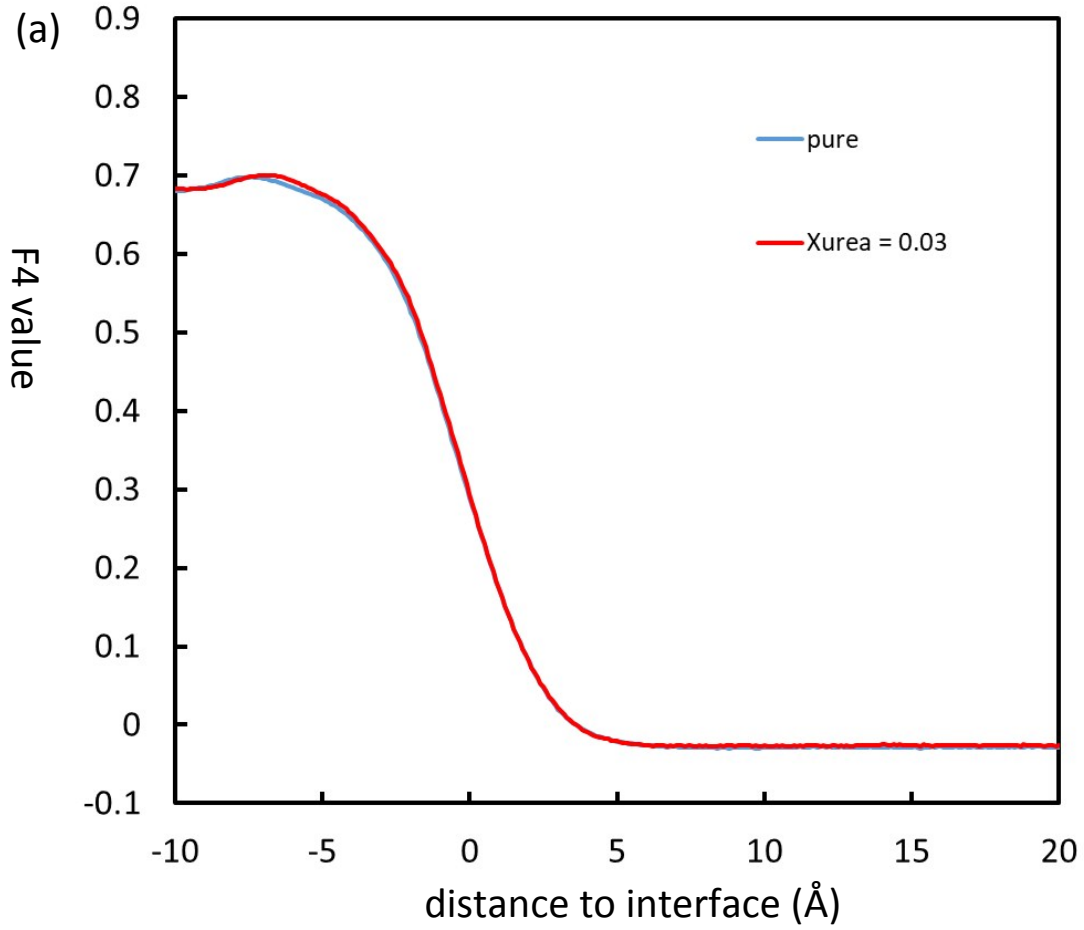
(a)
F4 value
0.9
0.8
0.7
0.6
0.5
0.4
0.3
0.2
0.1
0
-0.1
-10
-5
0
5
10
15
20
distance to interface (Å)
pure
Xurea = 0.03

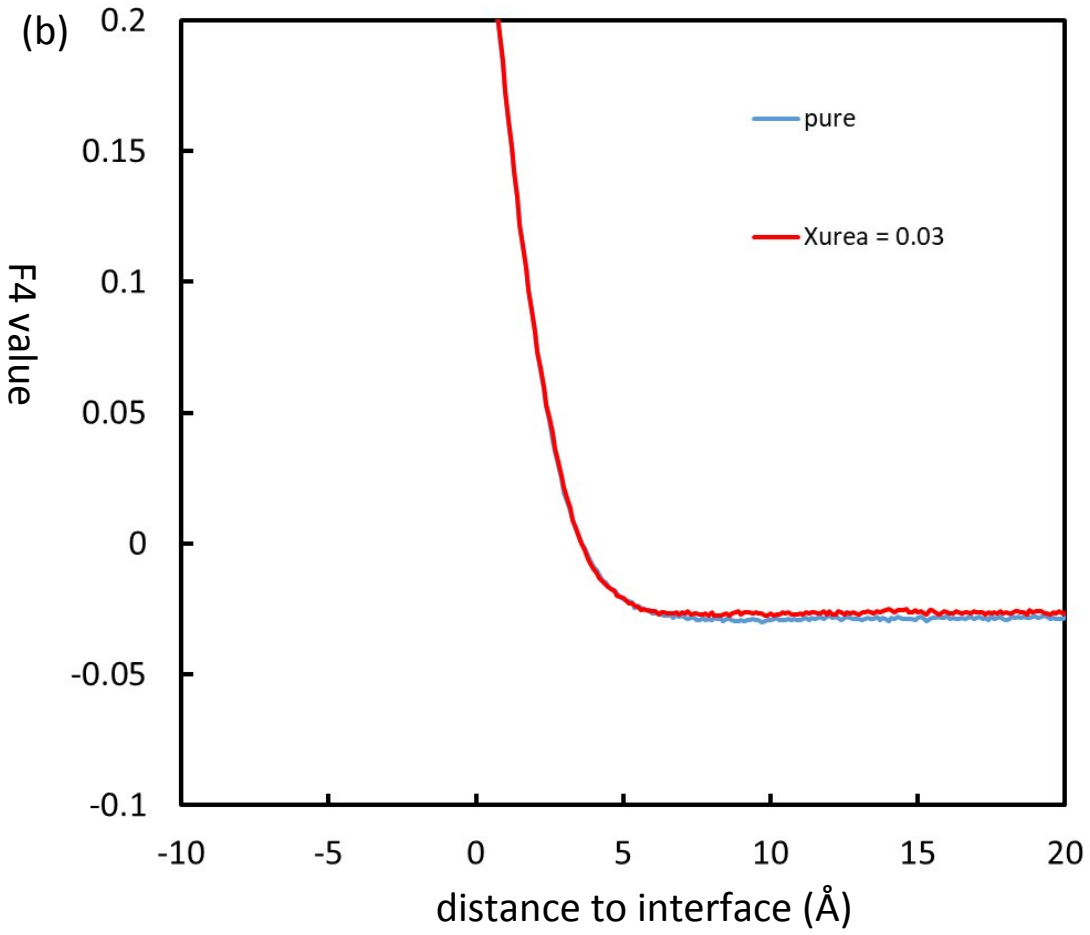

Figure S 36. The F4 distribution near the solid-liquid interface from hydrate equilibrium simulations (a). (b) Zoom in of the interface. Each line is an average of 4 data (2 interfaces from 2 independent simulations)

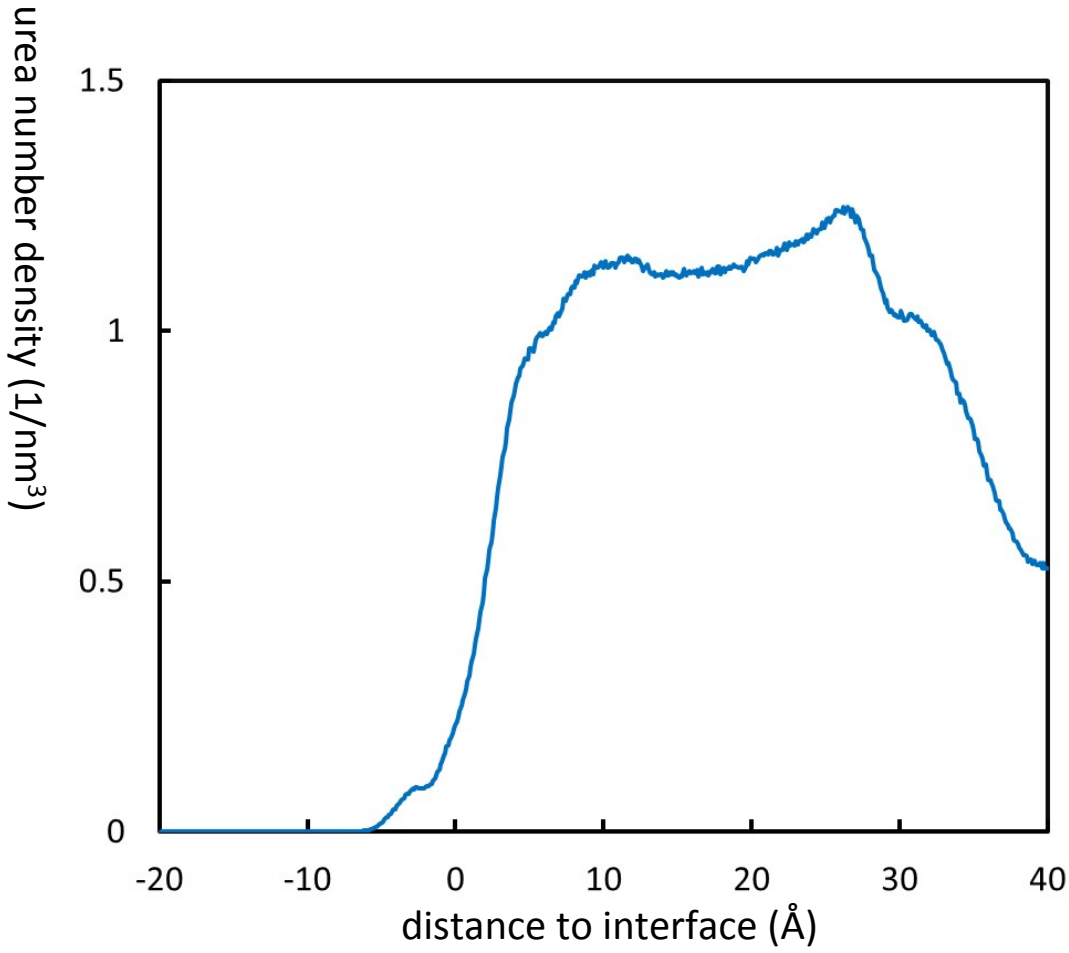

Figure S 37. Urea concentration distribution near the solid-liquid interface from hydrate growth simulations. The line is an average of 6 data (2 interfaces from 3 independent simulations)

a)

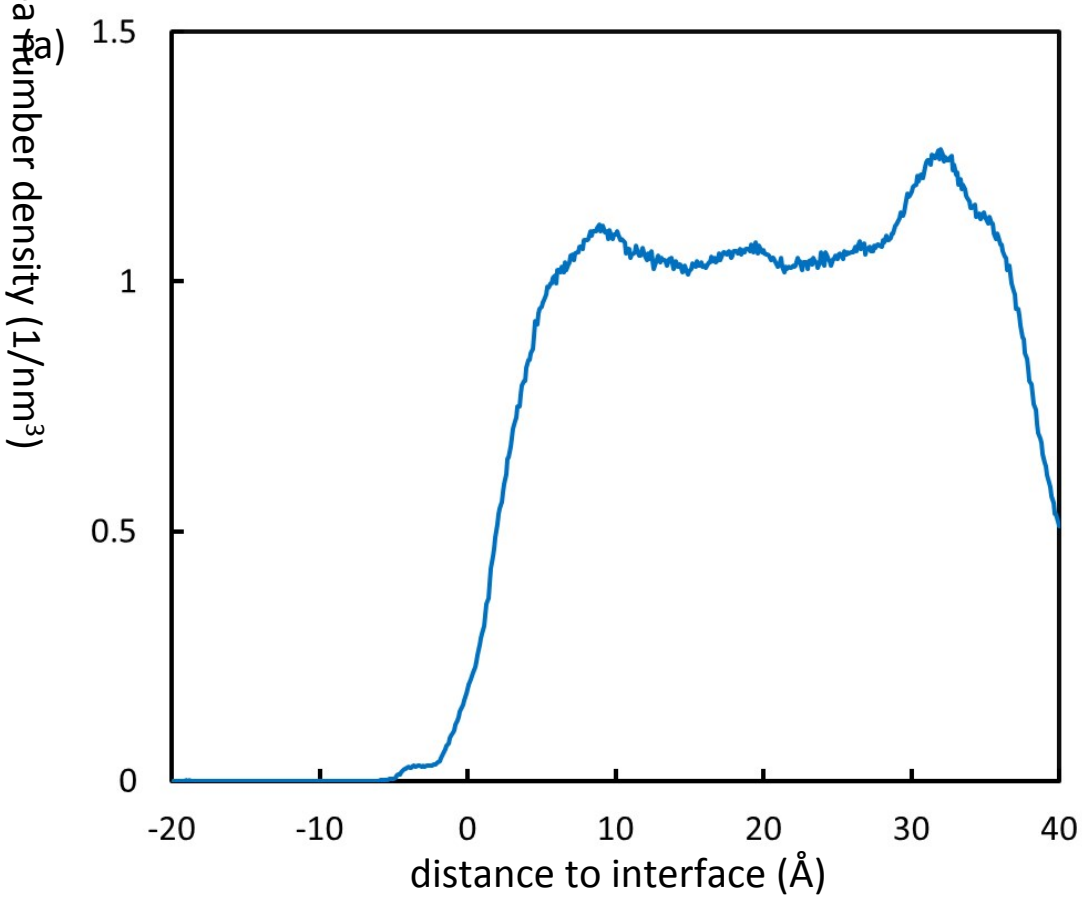
urea number density (1/nm3)
1.5
1
0.5
0
-20
-10
0
10
20
30
40
distance to interface (Å)

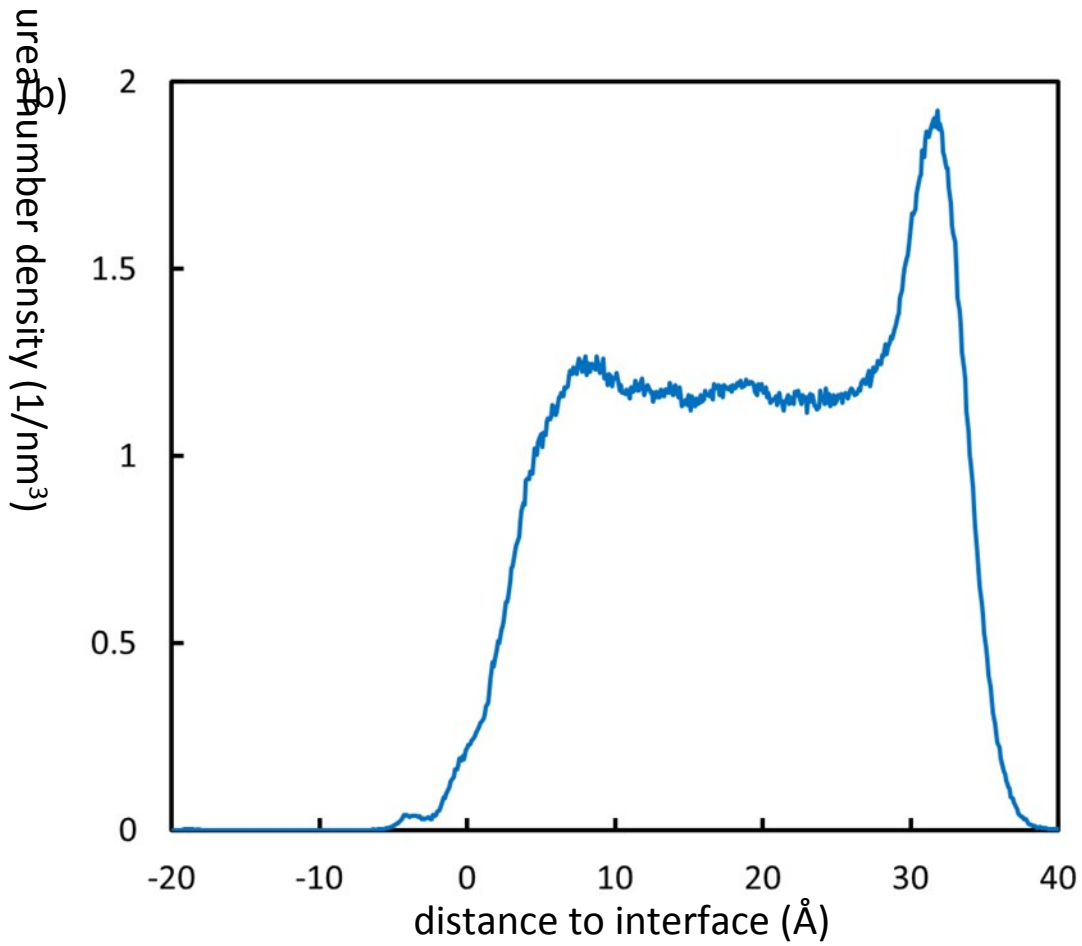

Figure S 38. Urea concentration distribution near the solid-liquid interface from hydrate equilibrium simulations (a). The line represent average of 4 data (2 interfaces from 2 independent simulations). (b) The urea concentration distribution near first solid-liquid interface of 283 K equilibrium simulation (run 1) during 300 ns to 400 ns.

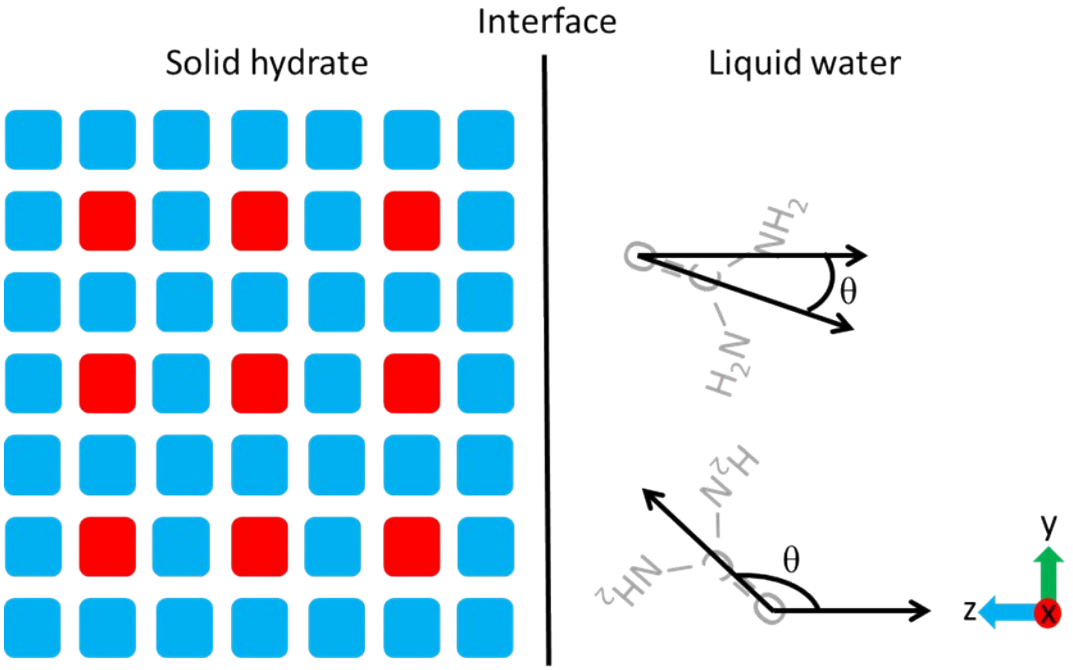

Figure S 39. Schematic diagram for determination of O=C direction near the solid-liquid interface.

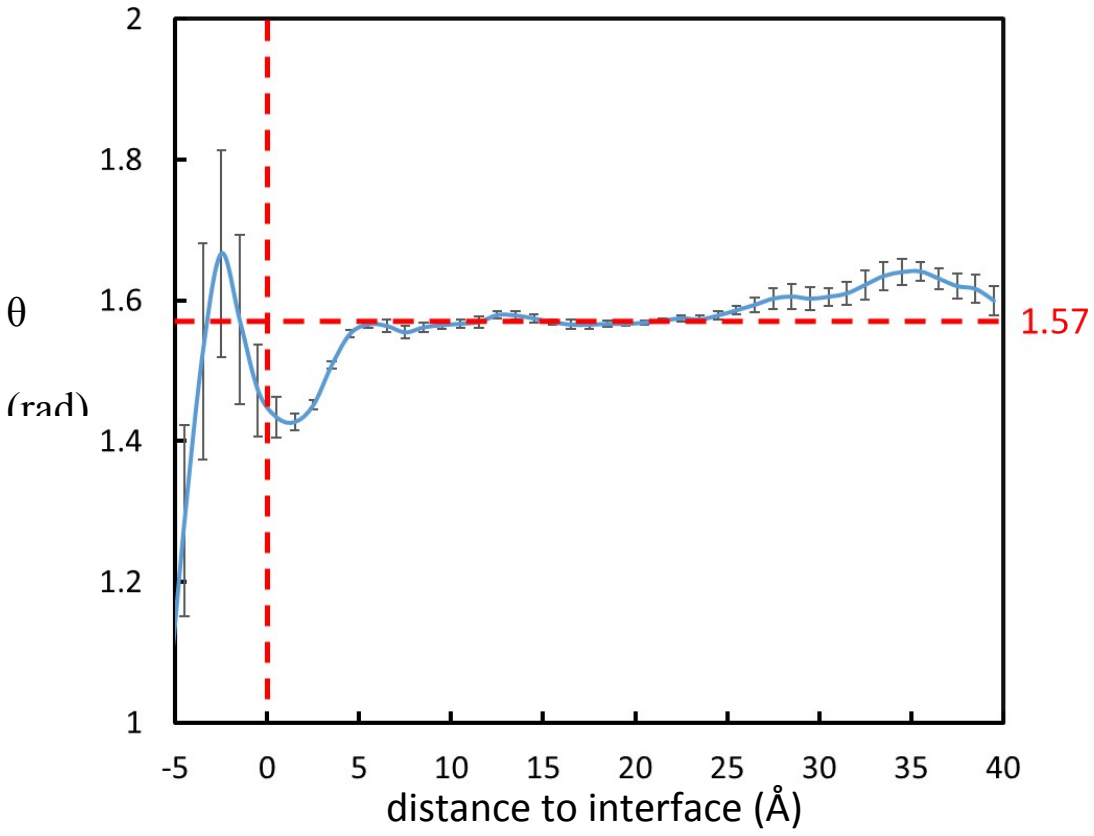

Figure S 40. The average angle θ between O=C of urea molecules and the surface normal near the solid–liquid interface from the hydrate growth simulations.

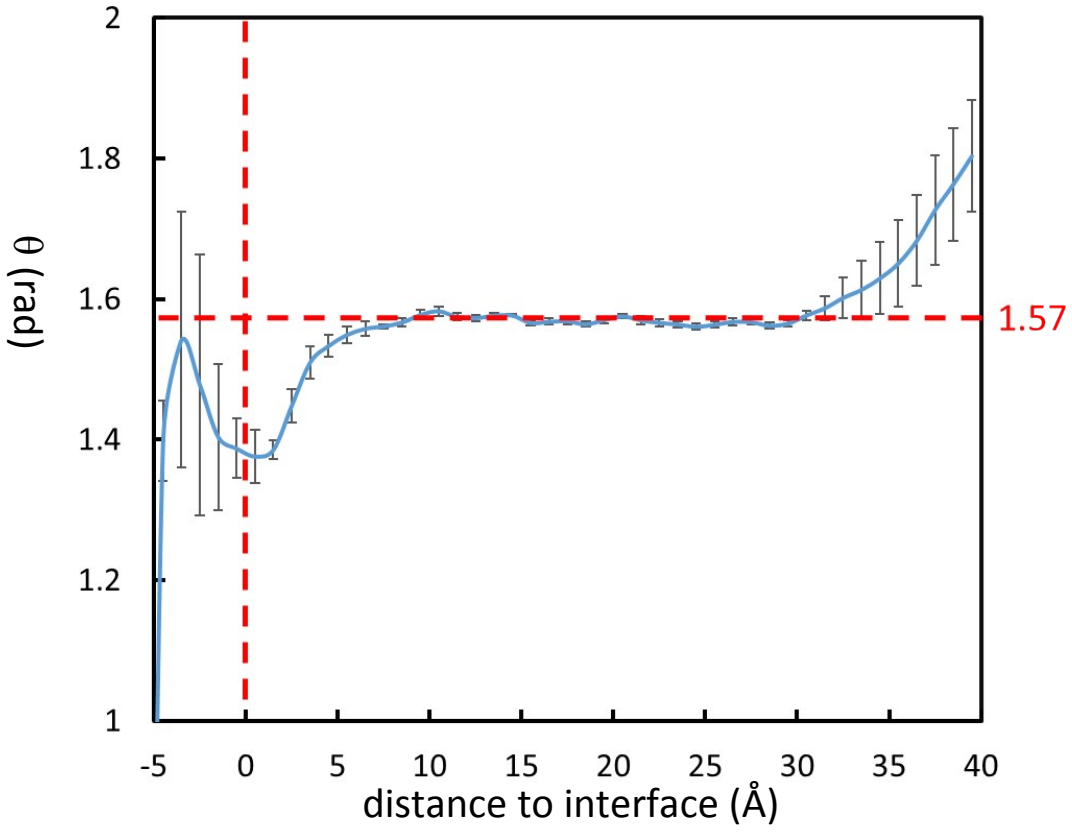

Figure S 41. The average angle θ between O=C of urea molecules and the surface normal near the solid–liquid interface from equilibrium simulations. The line is an average of 4 data (2 interfaces from 2 independent simulations)

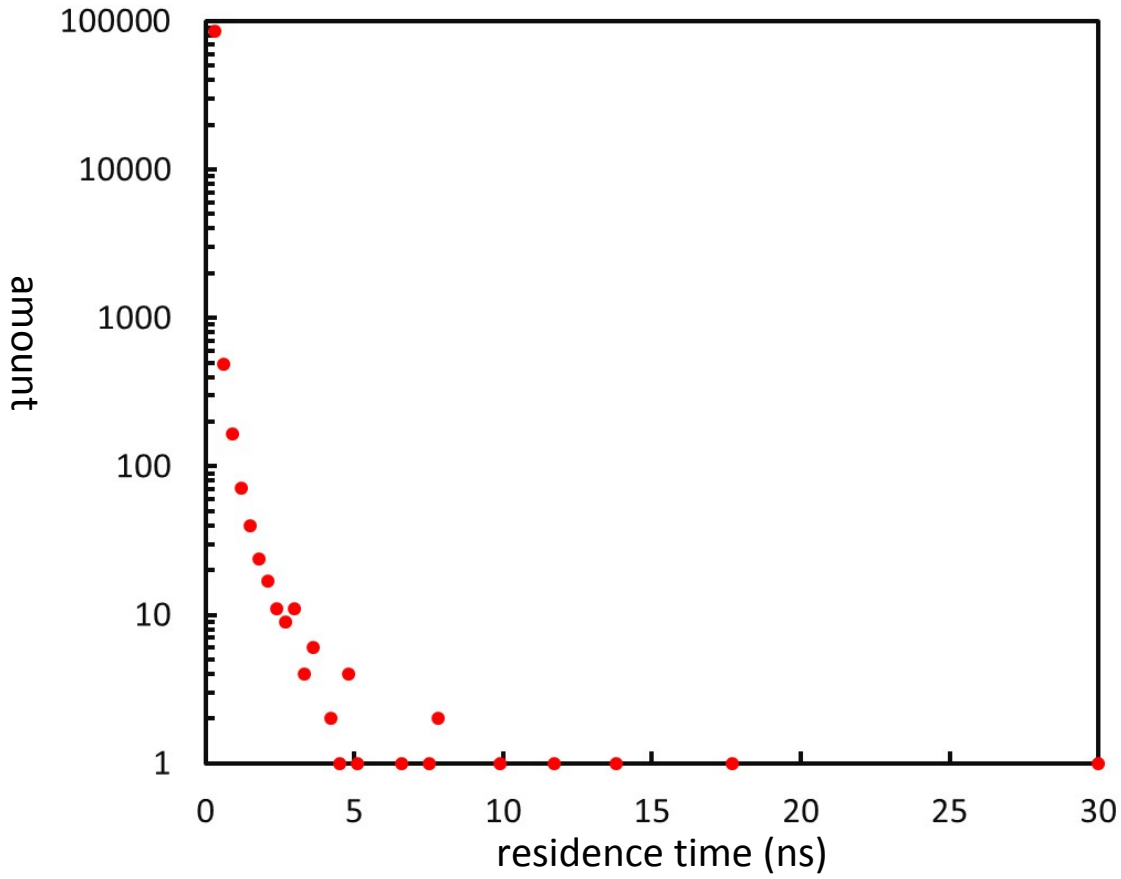

Figure S 42. The residence time of urea molecules near the surface (within 5 Å) of CO_2 hydrate. The time resolution on the x-axis is 300 ps.

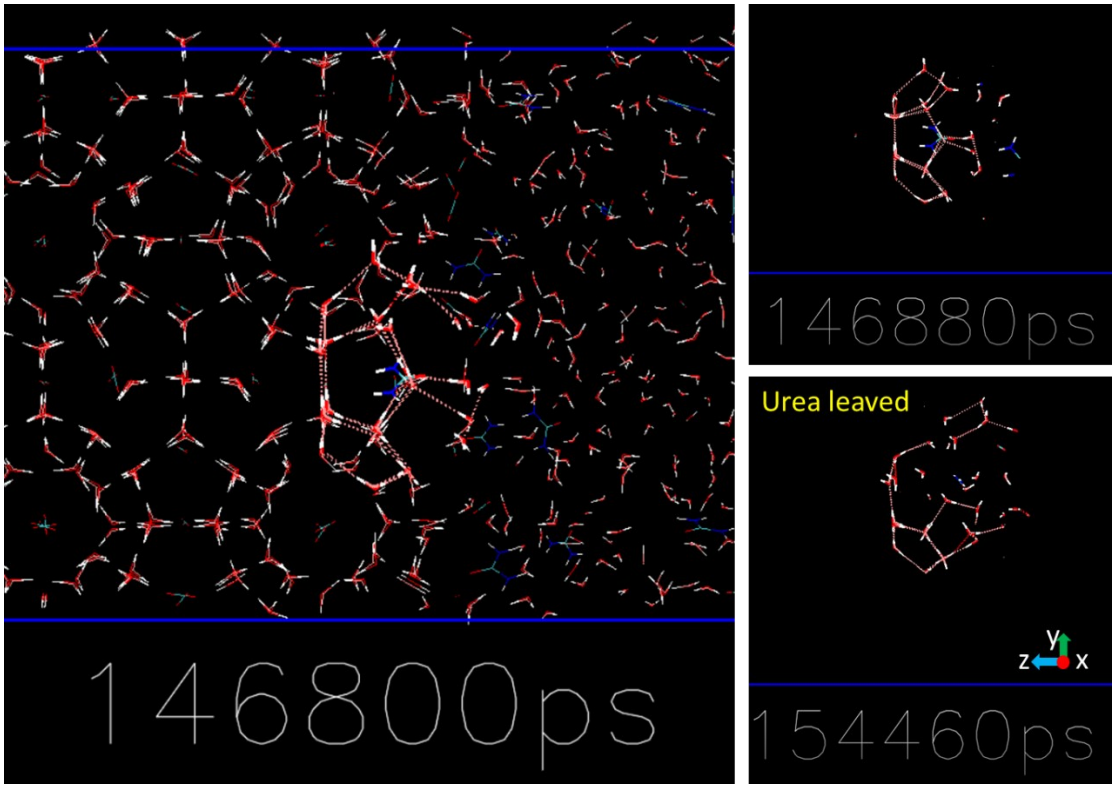

Figure S 43. Urea fits in an incomplete cage. (An example of the longest urea residence case of second interface of growth simulation (run 3).)

(a)

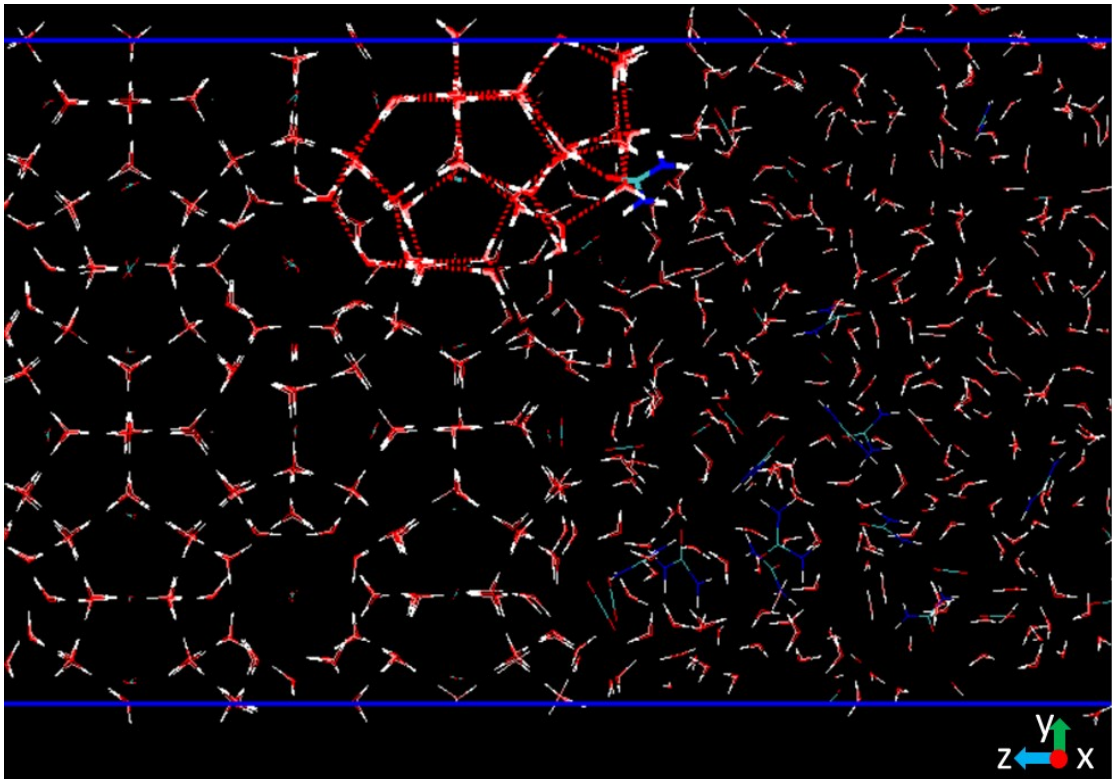

(b)

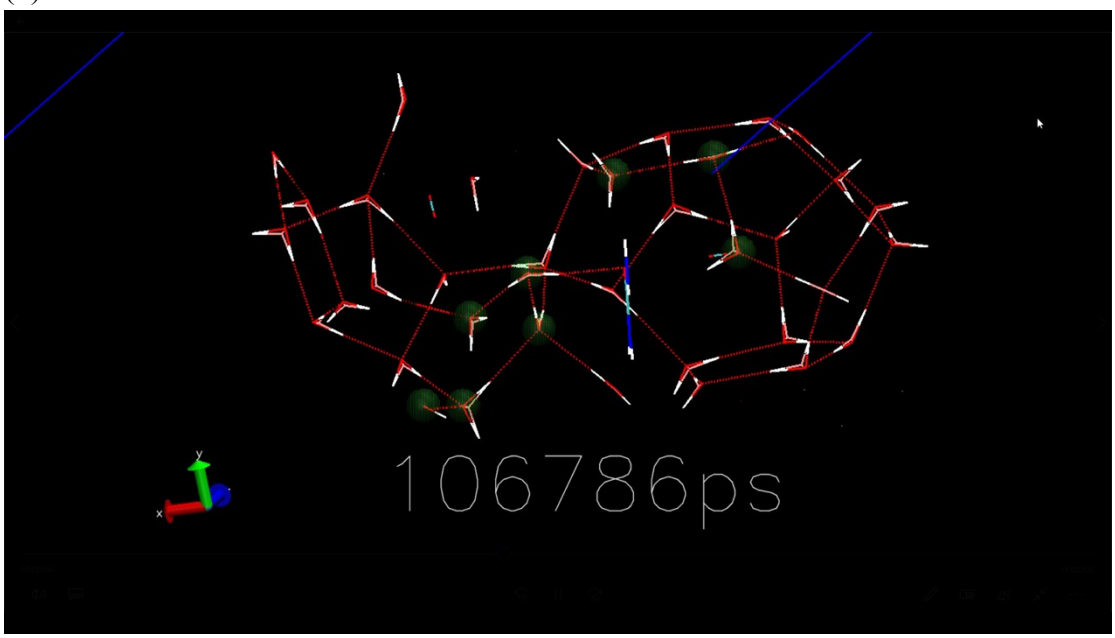

(c)

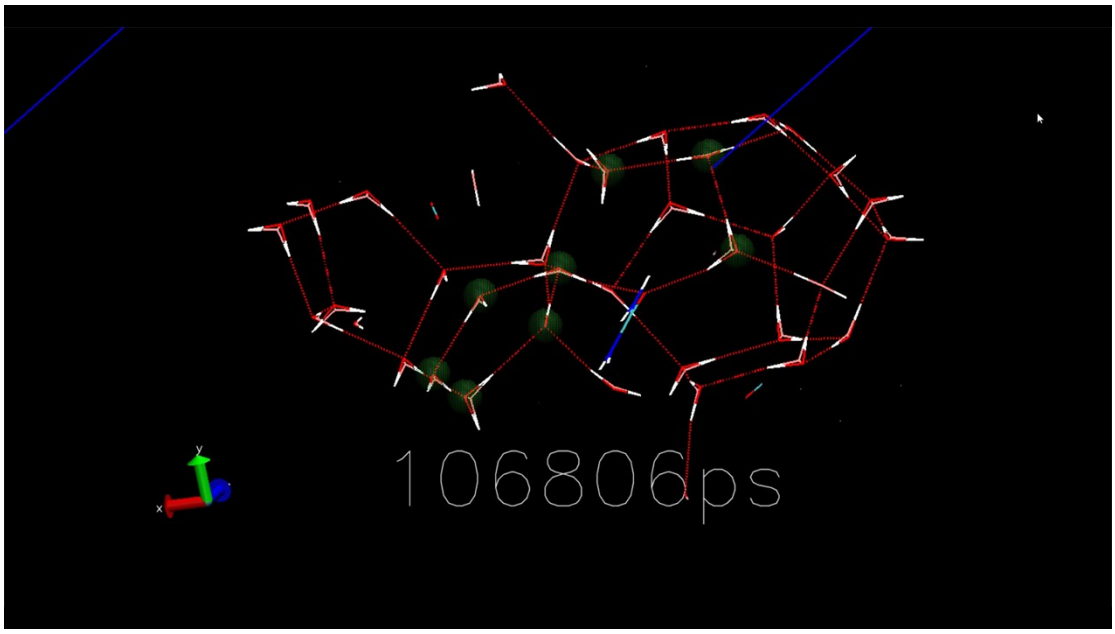

(d)

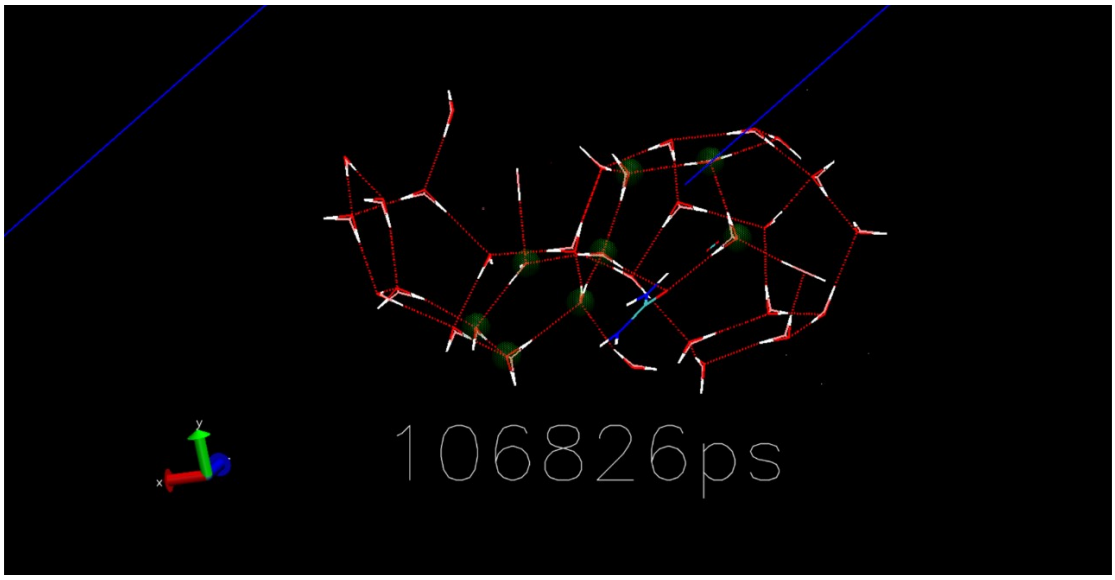

Figure S 44. The formation of pentagon rings with help of surface urea molecule. (a) Urea at hydrate surface (It's a 106826 ps snapshot from the hydrate growth simulation, run 1). (b) - (d) The snapshots of the evolution. The green shadow beads are water molecules on two 5-membered rings.

(a)

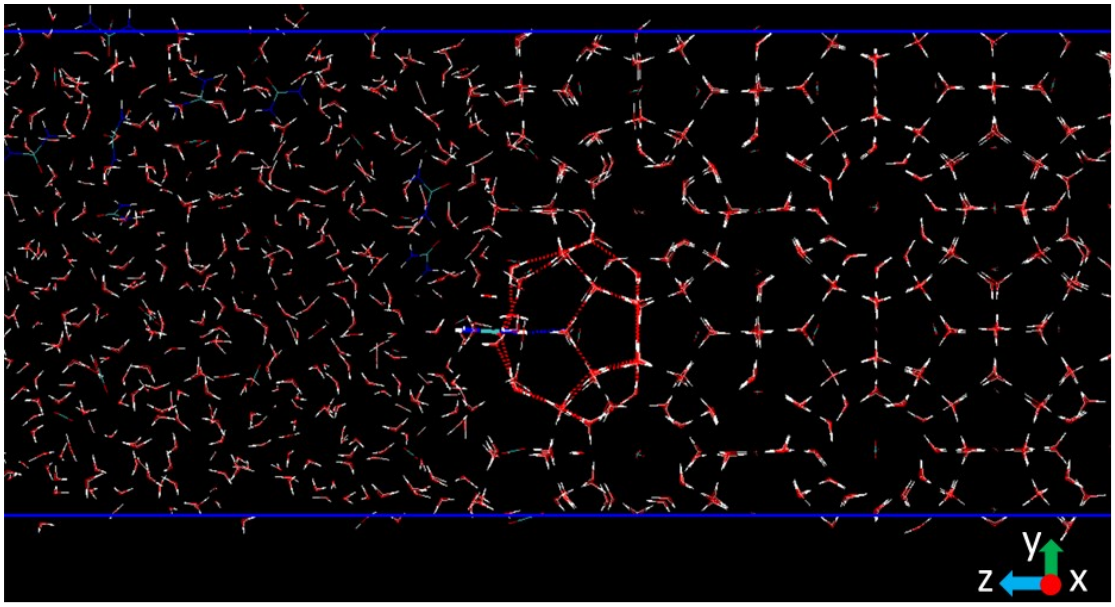

(b)

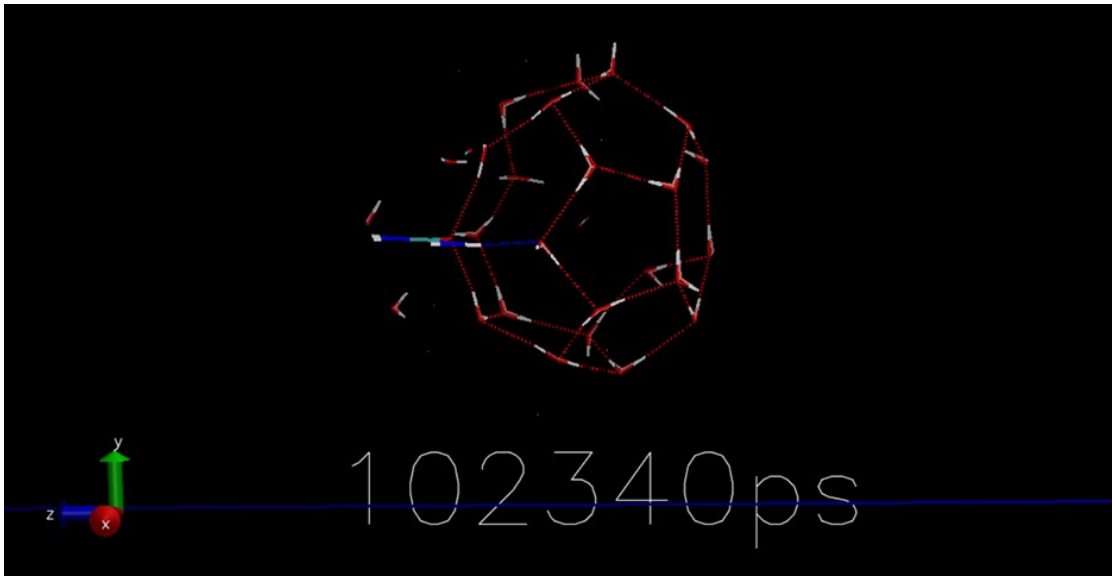

Figure S 45. Stabilization of the partial cage by urea. (a) Urea at hydrate surface (It's a 102340 ps snapshot from the hydrate growth simulation, run 1). (b) The snapshot of the urea-partial cage complex.

Table S 9. Maximum residence time of urea molecules and growth rate of each solid - liquid interface.

Solid–liquid interface	maximum residence time (ps)	Growth rate (Å/ns)
first interface of run 1	9672	0.139
second interface of run 1	7787	0.129
first interface of run 2	11690	0.115
second interface of run 2	13503	0.086
first interface of run 3	17528	0.143
second interface of run 3	29889	0.123
average	-	0.122

10. The CO_2 solubility in aqueous urea solution

The CO_2 solubility in aqueous urea solution is simulated using the initial structure shown in Figure S 46. The system contains two slabs. A gas phase of 750 CO_2 molecules, and a liquid phase of 1500 water molecules and 112 urea molecules (X_{urea} = 0.07). The simulations were conducted at 45 bar for 250 ns from 273 K to 298 K. The average amount of CO_2 molecules in the water phase in the last 200 ns equilibrium state is determined to be the solubility. The results are shown in Table S 10. The solubility in our simulation is about 30% - 40% higher than experimental data. The addition of urea would occupy the space and decrease number density of CO_2. However, it does not have an obvious influence on the ratio of CO_2 to water.

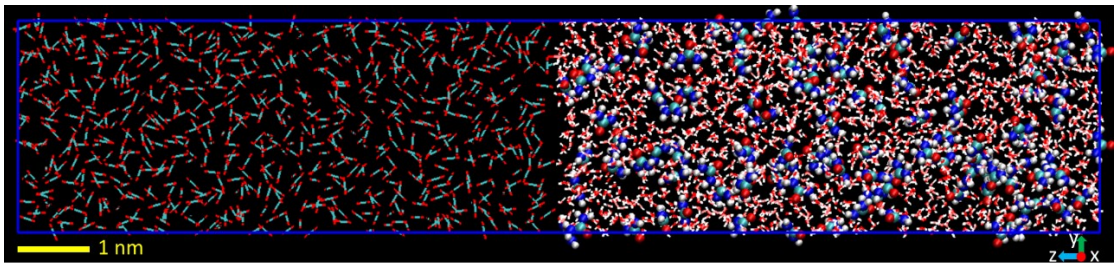

Figure S 46. The initial structure for CO_2 solubility in urea solution measurement.

Table S 10. The CO_2 solubility in water at 45 bar.

Temperature (K)	Mole fraction (CO_2/(CO_2+water))	Number density (1/nm^3)	Exp [24]
298	0.0296	0.957	0.0209
293	0.0313	1.013	
288	0.0334	1.081	0.0267
283	0.0368	1.187	
283 (X_{urea} = 0.07)	0.0365 (CO_2/(CO_2+water)) 0.0354 (CO_2/(CO_2+water+urea))	1.031	
278	0.0402	1.297	
273	0.0431	1.387	

11. The Self-diffusivity of water molecules

The water self-diffusivity at different temperatures and solution concentrations is summarized in Table S 12. The addition of urea increases water self-diffusivity at low temperatures (e.g., 280 K), but decrease water self-diffusivity at high temperatures (e.g., 333 K). While there is no experimental data conducted at 280 K, the results at 333 K is consistent with experimental observation.

Table S 11. Self-Diffusivity of water-CO_2-urea solution at 45 bar and 280 K.

system	water diffusivity (nm^2/ns)	CO_2 diffusivity (nm^2/ns) (standard error)
Pure water	0.626	
1500 water + 63 urea (X_{urea} = 0.04)	0.688	
1500 water + 60 CO_2 (X_{CO2} = 0.038)	0.458	0.449 (0.005)
1500 water + 63 urea + 60 CO_2	0.515	0.482

Table S 12. Water self-diffusivity at 1 bar and different temperature and different urea concentrations

Temp (K)	X_{urea}	diffusivity (nm^2/ps)	literature
280	0	0.000613	
	0.1	0.000675	
298	0	0.001135	0.0023 (exp) [25]
	0.1	0.001132	
333	0	0.002610	0.0047 (exp) [25], 0.0046 (simu) [26]
	0.1	0.002468	0.0018 (simu, X_{urea} = 0.126) [26]
	0.2	0.002108	

12. Reference

1. Pronk, S., et al., *GROMACS 4.5: a high-throughput and highly parallel open source molecular simulation toolkit.* Bioinformatics, 2013. **29**(7): p. 845-854.
2. Jones, J.E., *On the determination of molecular fields - II From the equation of state of a gas.* Proceedings of the Royal Society of London Series a-Containing Papers of a Mathematical and Physical Character, 1924. **106**(738): p. 463-477.
3. Toukmaji, A.Y. and J.A. Board, *Ewald summation techniques in perspective: A survey.* Computer Physics Communications, 1996. **95**(2-3): p. 73-92.
4. Allen, M.P. and D.J. Tildesley, *Computer Simulation of Liquids*. 1987: Oxford science publications.
5. Hoover, W.G., *CANONICAL DYNAMICS - EQUILIBRIUM PHASE-SPACE DISTRIBUTIONS.* Physical Review A, 1985. **31**(3): p. 1695-1697.
6. Parrinello, M. and A. Rahman, *POLYMORPHIC TRANSITIONS IN SINGLE-CRYSTALS - A NEW MOLECULAR-DYNAMICS METHOD.* Journal of Applied Physics, 1981. **52**(12): p. 7182-7190.
7. Abascal, J.L.F., et al., *A potential model for the study of ices and amorphous water: TIP4P/Ice.* Journal of Chemical Physics, 2005. **122**(23): p. 9.
8. Harris, J.G. and K.H. Yung, *CARBON DIOXIDES LIQUID-VAPOR COEXISTENCE CURVE AND CRITICAL PROPERTIES AS PREDICTED BY A SIMPLE MOLECULAR-MODEL.* Journal of Physical Chemistry, 1995. **99**(31): p. 12021-12024.
9. Jorgensen, W.L., D.S. Maxwell, and J. TiradoRives, *Development and testing of the OPLS all-atom force field on conformational energetics and properties of organic liquids.* Journal of the American Chemical Society, 1996. **118**(45): p. 11225-11236.
10. Duffy, E.M., D.L. Severance, and W.L. Jorgensen, *UREA - POTENTIAL FUNCTIONS, LOG-P, AND FREE-ENERGY OF HYDRATION.* Israel Journal of

Chemistry, 1993. **33**(3): p. 323-330.

11. Costandy, J., et al., *The role of intermolecular interactions in the prediction of the phase equ libria of carbon dioxide hydrates.* Journal of Chemical Physics, 2015. **143**(9): p. 8.
12. Miguez, J.M., et al., *Molecular dynamics simulation of CO2 hydrates: Prediction of three phase coexistence line.* Journal of Chemical Physics, 2015. **142**(12): p. 12.
13. Adisasmito, S., R.J. Frank, and E.D. Sloan, *HYDRATES OF CARBON-DIOXIDE AND METHANE MIXTURES.* Journal of Chemical and Engineering Data, 1991. **36**(1): p. 68-71.
14. Wiebe, R. and V.L. Gaddy, *The solubility of carbon dioxide in water at various temperatures from 12 to 40 degrees and at pressures to 500 atmospheres - Critical phenomena.* Journal of the American Chemical Society, 1940. **62**: p. 815-817.
15. Pinck, L.A. and M.A. Kelly, *The solubility of urea in water.* Journal of the American Chemical Society, 1925. **47**: p. 2170-2172.
16. Piana, S. and J.D. Gale, *Understanding the barriers to crystal growth: Dynamical simulation of the dissolution and growth of urea from aqueous solution.* Journal of the American Chemical Society, 2005. **127**(6): p. 1975-1982.
17. Swaminathan, S., B.M. Craven, and R.K. McMullan, *THE CRYSTAL-STRUCTURE AND MOLECULAR THERMAL MOTION OF UREA AT 12-K, 60-K AND 123-K FROM NEUTRON-DIFFRACTION.* Acta Crystallographica Section B-Structural Science, 1984. **40**(JUN): p. 300-306.
18. Davey, R., W. Fila, and J. Garside, *THE INFLUENCE OF BIURET ON THE GROWTH-KINETICS OF UREA CRYSTALS FROM AQUEOUS-SOLUTIONS.* Journal of Crystal Growth, 1986. **79**(1-3): p. 607-613.
19. Smith, L.J., H.J.C. Berendsen, and W.F. van Gunsteren, *Computer simulation of urea-water mixtures: A test of force field parameters for use in biomolecular simulation.* Journal of Physical Chemistry B, 2004. **108**(3): p. 1065-1071.
20. Chi-Hsiang Ho and Y.-P. Chen., *Measurement of Thermodynamics and Kinetics of Carbon Dioxide Hydrate in the Presence of Urea and 1,3-Cyclohexanebis(methylamine).* 2017, National Taiwan University.
21. Rodger, P.M., T.R. Forester, and W. Smith, *Simulations of the methane hydrate methane gas interface near hydrate forming conditions.* Fluid Phase Equilibria, 1996. **116**(1-2): p. 326-332.
22. Barnes, B.C., et al., *Two-component order parameter for quantifying clathrate hydrate nucleation and growth.* Journal of Chemical Physics, 2014. **140**(16): p. 6.

23. Yagasaki, T., M. Matsumoto, and H. Tanaka, *Molecular Dynamics Study of Kinetic Hydrate Inhibitors: The Optimal Inhibitor Size and Effect of Guest Species.* Journal of Physical Chemistry C, 2019. **123**(3): p. 1806-1816.
24. Valtz, A., et al., *Vapour-liquid equilibria in the carbon dioxide-water system, measurement and modelling from 278.2 to 318.2K.* Fluid Phase Equilibria, 2004. **226**: p. 333-344.
25. Krynicki, K., C.D. Green, and D.W. Sawyer, *PRESSURE AND TEMPERATURE-DEPENDENCE OF SELF-DIFFUSION IN WATER.* Faraday Discussions, 1978. **66**: p. 199-208.
26. Bennion, B.J. and V. Daggett, *The molecular basis for the chemical denaturation of proteins by urea.* Proceedings of the National Academy of Sciences of the United States of America, 2003. **100**(9): p. 5142-5147.